AGU PUBLICATIONS

JGR

Journal of Geophysical Research: Atmospheres

RESEARCH ARTICLE
10.1002/2016JD026116

**Key Points:**
- Precipitation properties around the Meghalaya Plateau in summer from 17 years of TRMM Precipitation Radar (PR) data
- Multiscale relationship between intraseasonal oscillation and diurnal variation
- Effects of land-atmosphere interaction and regional-scale orography on precipitation

**Supporting Information:**
- Supporting Information S1

**Correspondence to:**
H. Fujinami,
hatsuki@nagoya-u.jp

**Citation:**
Fujinami, H., Sato, T., Kanamori, H. & Murata, F. (2017). Contrasting features of monsoon precipitation around the meghalaya plateau under westerly and easterly regimes. *Journal of Geophysical Research: Atmospheres*, *122*. https://doi.org/10.1002/2016JD026116

Received 20 OCT 2016
Accepted 18 AUG 2017
Accepted article online 29 AUG 2017



# Contrasting Features of Monsoon Precipitation Around the Meghalaya Plateau Under Westerly and Easterly Regimes

**Hatsuki Fujinami[1], Tomonori Sato[2], Hironari Kanamori[1], and Fumie Murata[3]**

[1]Institute for Space-Earth Environmental Research, Nagoya University, Nagoya, Japan, [2]Faculty of Environmental Earth Science, Hokkaido University, Sapporo, Japan, [3]Faculty of Science and Technology, Kochi University, Kochi, Japan

**Abstract** Precipitation features around the Meghalaya Plateau, northeast India, during summer are investigated using a 17 year (1998–2014) high-spatial-resolution Tropical Rainfall Measuring Mission precipitation radar data set. Precipitation around the plateau fell into two distinct regimes based on the low-level wind direction that fluctuates on intraseasonal time scales over Bangladesh, windward of the plateau: a westerly regime (WR) and an easterly regime (ER). Under the WR, strong low-level onshore southwesterlies across Bangladesh encounter the plateau, and localized strong low-level southerlies running parallel to the Arakan Mountains (i.e., the barrier jet) also blow toward the plateau, concentrating convective unstable air onto its southern slopes. The low-level wind fields and large-scale upper level divergent fields promote frequent and intense orographic rainfall along the southern slopes due to forced uplift, generating high precipitation. In contrast, under the ER, strong southeasterlies that blow along the Gangetic Plain without encountering the plateau and subsidence inhibit upward motion around the plateau, resulting in low precipitation. Diurnal variations in precipitation significantly affect the daily precipitation around the plateau under both regimes. High rainfall frequency persists over the southern slopes between 2100 and 1200 LT of the next day under the WR, whereas modest rainfall frequency occurs between 0000 and 0600 LT under the ER, with a daytime minimum and nocturnal maximum in both regimes. The atmospheric boundary layer processes over Bangladesh regulate the wind speed and vertical structure of the low-level wind toward the plateau, with deceleration during daytime and acceleration at night (i.e., nocturnal jet) that result in the nocturnal rainfall maximum.

**Plain Language Summary** The Meghalaya Plateau of northeast India is one of the wettest places in the world. Extreme rainfall often causes flooding across the flat lowlands of Bangladesh to the south of the plateau. This study reveals the features contributing to this heavy rainfall and the mechanisms responsible using a 17 year (1998–2014) high-spatial-resolution spaceborne precipitation radar (TRMM-PR) data set and state-of-the-art atmospheric circulation data (ERA-Interim). Precipitation around the plateau is highly sensitive to whether strong low-level southerly monsoon winds from the ocean have westerly or easterly components (westerly and easterly regimes, respectively) over Bangladesh, windward of the plateau. Under the westerly regime, strong low-level southwesterlies blow over Bangladesh directly toward the plateau and localized strong low-level southerlies running parallel to the Arakan Mountains also blow toward the plateau. These winds concentrate moist air onto the southern slopes of the plateau, and rainfall occurs as the air is forced upward. The large rainfall amounts are caused by frequent heavy rain. In contrast, under the easterly regime, strong southeasterlies blow along the Gangetic Plain through northwestern Bangladesh and avoid the plateau, resulting in less frequent and lighter rain around the plateau.

## 1. Introduction

During the boreal summer, the large-scale meridional land-sea thermal contrast between South/Southeast Asia and the Indian Ocean maintains the prevailing strong moist low-level westerly/southwesterly flow over the Bay of Bengal (Li & Yanai, 1996; Ueda & Yasunari, 1998). The prevailing wind tends to turn northward when it reaches Bangladesh (Figure 1a). The Meghalaya Plateau is located in northeast India near the Bangladesh border. To its south, the flat lowlands of Bangladesh extend south to the Bay of Bengal, surrounded by mountainous terrain to the east and west. Although the height of this terrain is typically below 2,000 m, the topographic features around Bangladesh effectively act as a natural duct to guide strong and moist low-level southerlies from the Bay of Bengal toward the north. The Meghalaya Plateau, with a

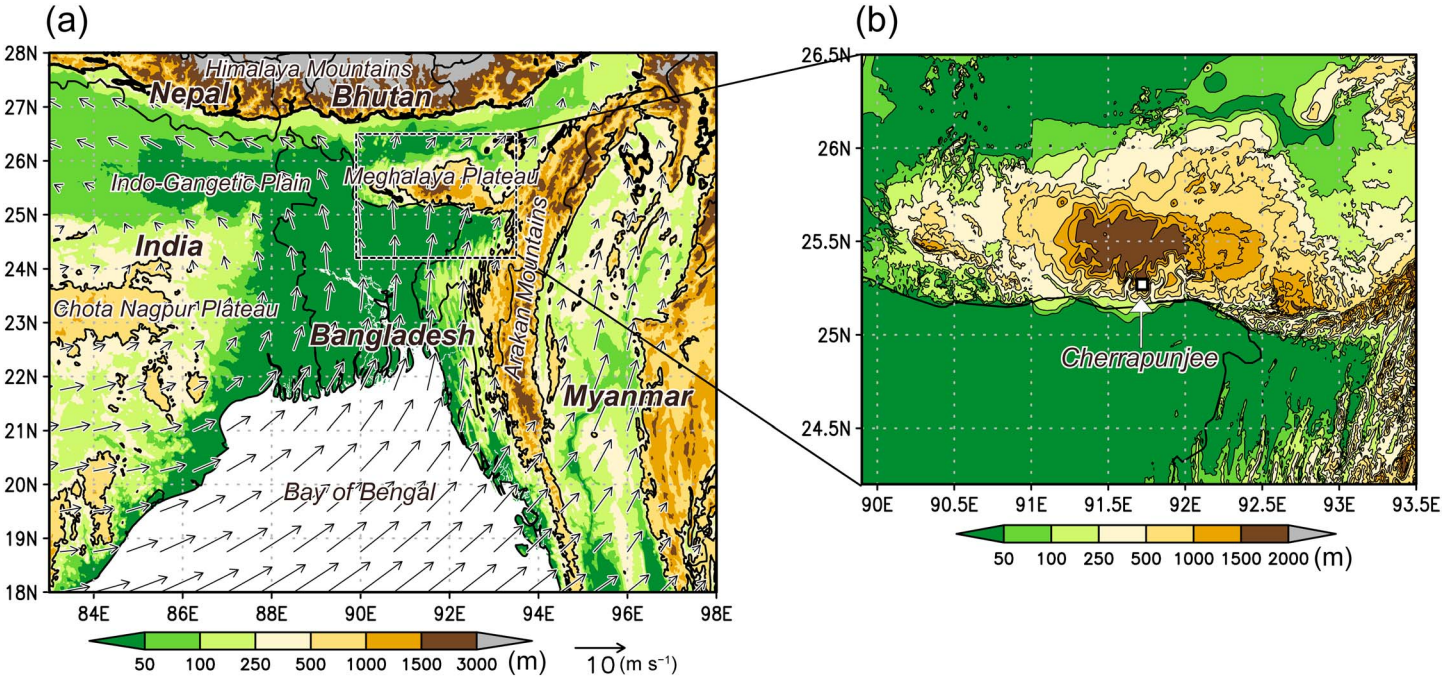


**Figure 1.** (a) Topography of the study area (shading) and climatological mean (1979–2014) wind fields at 925 hPa during summer (vectors). The 500 m topographic contour is shown by a thin solid line. (b) As in Figure 1a but around the Meghalaya Plateau. The white square over the southern slopes of the plateau indicates the location of Cherrapunjee station (25.25°N, 91.73°E). The figures were produced using GTOPO30 data provided by the United States Geological Survey (USGS).

maximum elevation of approximately 2,000 m, is the first orographic barrier to the low-level moist southerlies from the Bay of Bengal. This situation provides favorable conditions for high precipitation around the plateau. Indeed, the world record for the highest annual precipitation (26,461 mm) was recorded at Cherrapunjee (25.25°N, 91.73°E) in the southern part of the plateau (Figure 1b). The extreme precipitation around the plateau often causes flooding, especially over northeastern Bangladesh during the summer (Murata et al., 2007, 2008).

Intraseasonal oscillations (ISOs) are the dominant modes of atmospheric fluctuation over the tropics and the Asian monsoon region (Annamalai & Slingo, 2001; Chen & Chen, 1993; Goswami & Mohan, 2001; Krishnamurti & Ardanuy, 1980; Yasunari, 1979). High and low precipitation phases are often referred to as active and break phases, respectively. The ISOs typically have large-scale spatial structures and propagating characteristics in the atmospheric circulation fields and convection. Changes in atmospheric circulation due to the ISOs provide contrasting atmospheric environments for the genesis of tropical cyclones and monsoon lows (Goswami et al., 2003; Hatsuzuka et al., 2014; Hatsuzuka & Fujinami, 2017; Kikuchi & Wang, 2010; Krishnamurthy & Ajayamohan, 2010; Yanase et al., 2012) as well as diurnal variation in precipitation and orographic precipitation (Fujinami & Yasunari, 2001; Singh & Nakamura, 2010; Shrestha et al., 2012; Sato, 2013).

The precipitation over the southern slopes of the Meghalaya Plateau exhibits a pronounced quasi-biweekly/submonthly intraseasonal oscillation (Fujinami et al., 2014; Murata et al., 2008; Sato, 2013). The rainfall ISO is associated with the alternation of low-level zonal wind between westerly and easterly flows around the Gangetic Plain on the same time scales. In the active (break) phase, southwesterly (southeasterly) total column water vapor flux, which strongly depends on the low-level wind fields, covers the Bangladesh-Meghalaya Plateau region and induces a significant increase (decrease) in water vapor flux convergence, resulting in enhanced (reduced) rainfall over the region (Fujinami et al., 2011). The passage of a westward moving anticyclonic (cyclonic) circulation anomaly, which is a component of $n = 1$ equatorial Rossby waves (e.g., Kiladis et al., 2009), over the Bay of Bengal induces the enhancement of westerly (easterly) flow along the Gangetic Plain.

Cloud and precipitation over the southern part of the Meghalaya Plateau also show a diurnal variation. Unlike typical diurnal variations over land, in which the maximum rainfall appears between noon and early evening

because of surface heating during the day, nocturnal rainfall dominates around the southern slopes of the plateau (Hirose et al., 2008; Ohsawa et al., 2001; Romatschke & Houze, 2011; Sato, 2013; Terao et al., 2006). Kataoka and Satomura (2005) examined the diurnal variation of precipitation in the active rainfall period of 14–21 June 1995 over northeastern Bangladesh near the southern slopes of the Meghalaya Plateau using a nonhydrostatic mesoscale model. The stronger low-level southwesterlies at night compared with those in daytime over Bangladesh were responsible for triggering the maxima of precipitation from late night to early morning around the southern slopes of the plateau, rather than the katabatic mountain wind often used to explain nighttime precipitation maxima along the windward slopes of mountains (Bhatt & Nakamura, 2006; Ohsawa et al., 2001). Terao et al. (2006) examined the diurnal variation of wind in some locations over Bangladesh using in situ rawinsonde and pilot balloon observational data in the break phase of rainfall in the summers of 2000 and 2001 over Bangladesh. Southerlies accelerate in the evening in the lower troposphere, and the wind direction exhibits a clockwise change at night, indicative of the behavior of a nocturnal jet (Blackadar, 1957; Van de Wiel et al., 2010). They also discussed the possible effect of the nighttime enhancement of low-level wind on the early morning peak of rainfall over northeastern Bangladesh. Using a cloud-resolving model, Sato (2013) also pointed out the importance of the nocturnal low-level jet (LLJ) appearing around 900 hPa for enhancing orographic rainfall around the southern slopes of the Meghalaya Plateau in summer 2004. The direction of the LLJ varies with the diurnal cycle, which accelerates the preexisting southwesterly flow near the plateau between 1800 and 0600 LT in the active rainfall phase of the submonthly ISO. Thus, the behavior of low-level wind on the windward side of the plateau and below the height of the plateau is critical in regulating orographic precipitation around the Meghalaya Plateau on both intraseasonal and diurnal time scales.

Tropical Rainfall Measuring Mission (TRMM) Precipitation Radar (PR) data have provided much useful information on precipitation features in areas of the Asian monsoon region with complex terrain (Barros et al., 2004; Biasutti et al., 2012; Fujinami et al., 2005; Hirose & Nakamura, 2005; Hirose et al., 2008; Nesbitt & Anders, 2009; Romatschke et al., 2010; Shrestha et al., 2012; Singh & Nakamura, 2010; Takahashi et al., 2010). However, previous studies have not considered the detailed features of rainfall, including diurnal variations, related to the ISO around the Meghalaya Plateau using TRMM PR data. Multiyear (1998–2014) TRMM PR data can be used to investigate such issues climatologically over complex regional-scale topography, such as that of the Meghalaya Plateau, with high vertical and horizontal precision.

Therefore, the purpose of this study is to describe the precipitation characteristics around the Meghalaya Plateau under the different low-level wind regimes associated with the ISO using a 17 year high-spatial-resolution TRMM PR data set. The three-dimensional atmospheric circulation responsible for the different precipitation regimes is also investigated. We further present detailed features of the diurnal rainfall variation around the plateau. The diurnal variation of a low-level jet over topographic features around Bangladesh is examined to understand the diurnal variation of precipitation over the southern slopes.

## 2. Data and Methods

We used ERA-Interim reanalysis (Dee et al., 2011) on a 0.75° × 0.75° grid, which is produced by the European Centre for Medium-Range Weather Forecasts (ECMWF), to investigate summer (June–August) synoptic-scale atmospheric circulation for the period 1979–2014. This reanalysis has a finer horizontal resolution and more vertical levels below 850 hPa (i.e., seven levels) than first generation reanalyses such as the National Center for Environmental Prediction/National Center for Atmospheric Research reanalysis. Thus, the ERA-Interim reanalysis is well suited to the study of the Bangladesh-Meghalaya region, which is surrounded by complex terrain with an elevation typically below 2,000 m. We selected the 925 hPa level zonal wind ($u$) as representative of the low-level wind regimes because the climatological summer maximum horizontal wind speed in the lower troposphere appears at 925 hPa (~700 m above sea level) from the head of the Bay of Bengal to Bangladesh (see Figure 6). The reason for focusing on the zonal wind is explained in subsection 3.1. Daily and 6-hourly data were used to generate the composite patterns related to the wind regimes and diurnal variation, respectively.

We also used the TRMM 2A25 version 7 data (Iguchi et al., 2000) for 17 summers (1998–2014) to study precipitation characteristics around the Meghalaya Plateau. Such long-term data are useful for examining the precipitation features in a regional domain because the increase in sample number reduces sampling

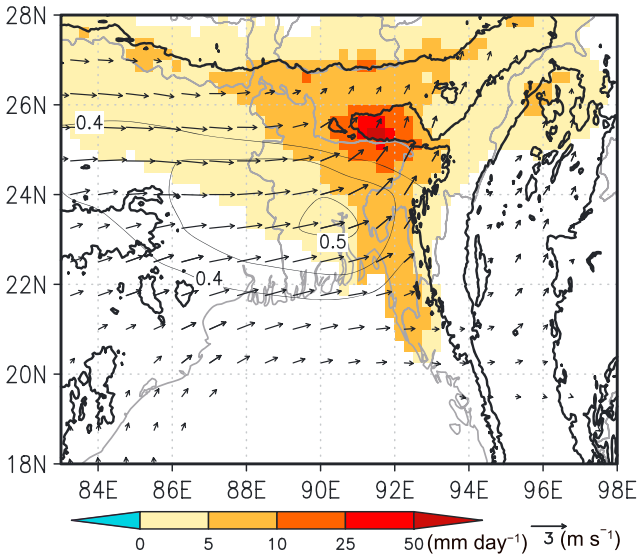


**Figure 2.** Regression patterns of summer precipitation (shading) and horizontal wind (vectors) at 925 hPa based on standardized daily precipitation time series at the grid point (25.3°N, 91.7°E) closest to Cherrapunjee for 29 years (1979–2007). Only areas of rainfall that are statistically significant at the 99% level are shaded, as determined by correlation coefficients based on 624 degrees of freedom (see text for details). Note that the precipitation data (APHRODITE) do not cover the ocean. Wind vectors are plotted where either the *u* or *v* component exceeds the 99% local confidence level. The thick solid line indicates the 500 m topographic contour. Thin solid lines show the correlation coefficient between rainfall at the grid point (25.3°N, 91.7°E) closest to Cherrapunjee and the zonal wind component (*u*) at 925 hPa. The correlation contours of 0.4, 0.45, and 0.5 are only shown to indicate the location of its maximum.

errors. The TRMM PR is the first spaceborne radar that can provide three-dimensional maps of the structure of precipitation systems (Kummerow et al., 1998, 2000). The original horizontal resolution was 4.3 km at nadir but was changed to 5.0 km after an orbital boost maneuver in 2001. The vertical resolution is 250 m. The minimum detectable rainfall rate of the PR is about 0.5 mm $h^{-1}$. We used the near-surface rain rate to examine the spatial distribution of rainfall and to calculate the rainfall frequency (number of rain samples as a percentage of the total number of samples) and rain intensity (mean near-surface rain rate during rain events). We used the rain flag data from TRMM PR product 2A25 for rain-type classifications. The PR algorithm classifies the rain pixels into three categories: convective, stratiform, and others. To obtain precipitation characteristics related to the ISO and diurnal variation, gridded data were compiled from the instantaneous data on a 0.05° × 0.05° latitude-longitude resolution grid over 1 h intervals. Modulation of the precipitation characteristics around the Meghalaya Plateau under different wind regimes was revealed through composite analyses based on the data set.

We also used the APHRODITE (Asian precipitation - highly resolved observational data integration toward evaluation of water resources) daily rainfall data set (Yatagai et al., 2009, 2012) to examine the statistical relationship between day-to-day variation of rainfall and low-level wind fluctuations around the Meghalaya Plateau for the period 1979–2007 (29 years). The APHRODITE data set is a high-resolution (0.25° × 0.25°) daily precipitation data set that covers the Asian landmass. The data set is created primarily from data obtained from a dense rain gauge observation network. APHRODITE includes two rain gauge stations, Cherrapunjee and Shillong (25.6°N, 91.9°E), on the Meghalaya Plateau (Yatagai et al., 2009). A comparison of rainfall time series from summer 2004 between the rain gauge observations at Cherrapunjee (Murata et al., 2008) and APHRODITE at the grid point (25.3°N, 91.7°E) closest to Cherrapunjee shows similar variation in the timing of the ISO signals, although the absolute value of the gauge-based observation is about 1.5 times that from APHRODITE (figure not shown) in the active phase of the ISO. Thus, the APHRODITE data are of good enough quality to represent the ISO activity around the Meghalaya Plateau. Hereafter, we consider the nearest grid cell to Cherrapunjee as Cherrapunjee.

We used the GTOPO30 data provided by the United States Geological Survey (USGS) with a spatial resolution of 0.008° × 0.008° for the surface elevation around the Meghalaya Plateau. We also used the data averaged over 0.05° × 0.05° grid cells for the topography for large areas. Essentially, we display the topography from the GTOPO30 together with atmospheric circulation fields from ERA-Interim to show a realistic relationship between the height of the Meghalaya Plateau and the low-level atmospheric circulation. The ERA-Interim topography represents the Meghalaya Plateau as separate from the Himalayas, but with a maximum height of 522 m that is only a third of its real value (see Figure 13).

## 3. Results

### 3.1. Westerly and Easterly Wind Regimes

First, in order to classify the wind regimes associated with precipitation variation, we examine the statistical relationship between summer precipitation in the southern part of the Meghalaya Plateau (Figure 1b) and low-level wind over the surrounding regions for the period 1979–2007 on a daily basis. We assembled the daily rainfall at Cherrapunjee, rainfall and horizontal wind at 925 hPa in every grid during summer, following the sequential order of the years from 1979 to 2007 to make a new data set (2668 days).

Figure 2 shows the regression pattern of precipitation and horizontal wind at 925 hPa regressed onto the standardized daily rainfall anomaly at Cherrapunjee from the APHRODITE data set during summer. The

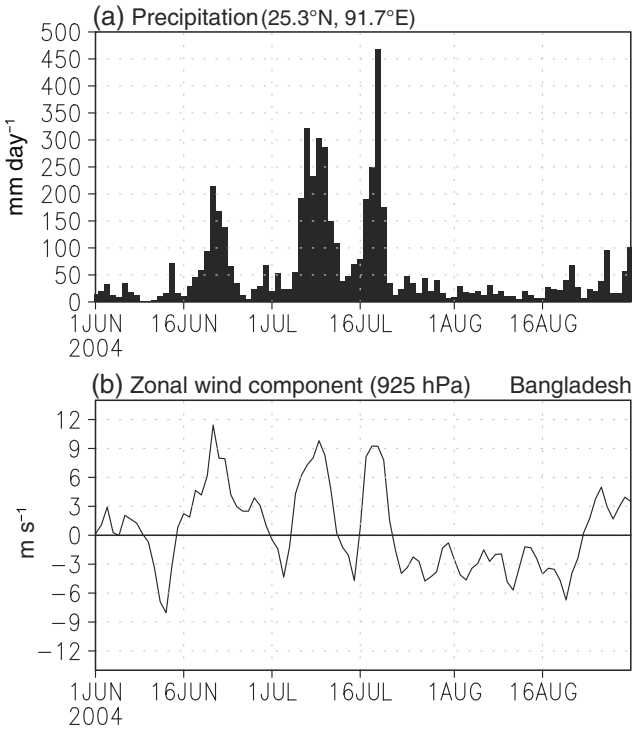


**Figure 3.** (a) Time series of precipitation at the grid point (25.3°N, 91.7°E) closest to Cherrapunjee in the summer of 2004. (b) As in Figure 3a but for zonal wind (*u*) at 925 hPa over the key area of Bangladesh. Positive and negative values mean westerly and easterly winds, respectively.

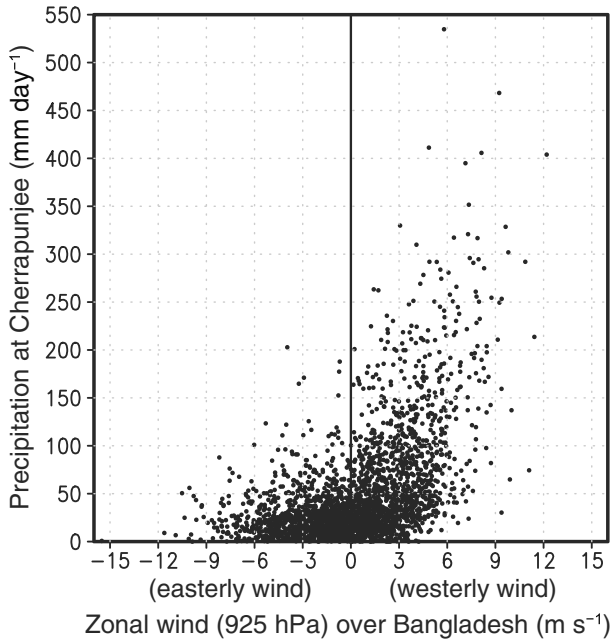


**Figure 4.** Scatterplot of summer daily mean zonal wind component (*u*) over the key area of Bangladesh and daily precipitation at the grid point (25.3°N, 91.7°E) closest to Cherrapunjee for the period from 1979 to 2007.

effective number of degrees of freedom for the precipitation time series at Cherrapunjee is approximately 624, taking the lag-1 autocorrelation of the time series (0.62) into account (Trenberth, 1984). The regression pattern in precipitation and wind fields captures the characteristic anomaly fields of the composite difference between active and break phases of the submonthly ISO around Bangladesh well (Fujinami et al., 2011, 2014). Statistically significant positive rainfall anomalies extend over Bangladesh, northeastern India, Nepal, Bhutan, and northwestern Myanmar. High anomalous values (>25 mm d$^{-1}$) are observed around the southern slopes of the plateau with the maximum exceeding 50 mm d$^{-1}$ in Cherrapunjee. Anomalous values of more than 5 mm d$^{-1}$ are observed to the south of the Meghalaya Plateau along the western side of the Arakan Mountains and over the foothills of the Himalayas around Bhutan.

Westerly (easterly) wind anomalies at 925 hPa dominate the Gangetic Plain during positive (negative) daily rainfall anomalies on the southern slopes of the Meghalaya Plateau, while southwesterly wind anomalies are observed in a limited area to the south of the plateau along the western side of the Arakan Mountains. The magnitude of the zonal wind anomalies is larger than that of the meridional wind component in the windward area of the plateau around Bangladesh. Thus, zonal wind is used as an index to classify two distinct precipitation regimes over the plateau. The rectangular region (23.25°N–24°N, 89.25°E–91.5°E) over the lowlands of central Bangladesh where a maximum positive correlation between the rainfall at Cherrapunjee and zonal wind at 925 hPa appears (hereafter, referred to as the key area) is used to determine the wind regimes for a detailed examination of precipitation around the Meghalaya Plateau. Note that climatological summer mean wind fields at 925 hPa are southerlies with almost no zonal wind component (Figure 1a); these southerlies are essential to the development of high precipitation over the southern slope. However, around the key area, the zonal wind fluctuation is more closely tied to precipitation fluctuations related to the ISO in the southern part of the plateau, rather than to the meridional wind component. Detailed dynamics of the low-level wind fields, including the meridional wind component, that regulate precipitation around the plateau will be presented in the following subsections.

Figure 3 shows an example of a rainfall time series from Cherrapunjee and of the 925 hPa zonal wind component in the key area in summer 2004. The rainfall series exhibits a high-amplitude intraseasonal oscillation over the submonthly time scale from June to mid-July, which is consistent with the results of Murata et al. (2008) and Sato (2013). The zonal wind also exhibits an intraseasonal oscillation over the same time scale (Figure 3b). The high rainfall periods (i.e., the active phase) correspond well to the westerly wind regime, whereas low precipitation (i.e., the break phase) is observed under the easterly wind regime. As in 2004, in almost all years, large zonal wind fluctuations occur on a submonthly time scale around Bangladesh (Fujinami et al., 2014).

To show the zonal wind-precipitation relationship in the total fields, the scatter diagram of the 925 hPa daily mean zonal wind component over the key area and precipitation in Cherrapunjee is shown in

Figure 4. Most of the high precipitation rates of more than 100 mm $d^{-1}$ occur in Cherrapunjee when there is a westerly wind over Bangladesh. Zonal wind and precipitation have a positive linear relationship. In contrast, in cases with an easterly wind, the linear relationship appears to break up. Precipitation is generally less than 50 mm $d^{-1}$, although it exceeds 100 mm $d^{-1}$ infrequently.

Thus, from the results shown in Figures 2–4, the low-level zonal wind component windward of the plateau is closely associated with the different precipitation regimes related to the ISO around the Meghalaya Plateau. In addition, the zonal wind anomalies related to the ISO in Figure 2 are concurrently observed across all layers of the troposphere over the Gangetic Plain (Murata et al., 2008; Fujinami et al., 2014). Thus, the low-level zonal wind fluctuation over the key area, as defined above, also captures the change of atmospheric circulation related to the ISO throughout the troposphere.

Therefore, we partitioned the daily time series of the 925 hPa zonal wind component over the key area for the period 1998–2014 in summer (1564 days) into a westerly regime (WR; 923 days) and an easterly regime (ER; 641 days) to investigate precipitation properties around the Meghalaya Plateau and the dynamics of atmospheric circulation regulating precipitation properties in the distinct wind regimes.

### 3.2. Synoptic Conditions

Figures 5a and 5b show composites of the rainfall and 925 hPa wind fields under the WR and ER. Characteristics of the spatial patterns under the WR and ER in the figures are nearly identical to those in the active and break phases of the ISO around the Bangladesh-Meghalaya Plateau regions, respectively (Fujinami et al., 2014). The WR is characterized by strong southwesterly winds from the Bay of Bengal toward the Meghalaya Plateau and high precipitation of more than 40 mm $d^{-1}$ over the southern slopes of the plateau. High precipitation also appears over the foothills of the Himalayas around the border between India and Bhutan. Precipitation of more than 10 mm $d^{-1}$ spreads over Bangladesh, northeastern India, and the countries along the southern slopes of the Himalayas. In contrast, under the ER, strong southeasterly winds from the Bay of Bengal blow over Bangladesh and avoid the Meghalaya Plateau, with low precipitation over the southern slopes of the plateau. As a whole, low precipitation is observed around the Gangetic Plain where high precipitation appears under the WR, while precipitation is enhanced over the Bay of Bengal. Both regimes show strong low-level southwesterlies over the Bay of Bengal, but they have an opposite zonal wind direction over Bangladesh. The spatial pattern of the difference in the wind fields and precipitation between the WR and ER (Figure S1) is similar to that in Figure 2, indicating high (low) precipitation around the Meghalaya Plateau in the case of westerly (easterly) flow around the Gangetic Plain.

The contrast in atmospheric circulation between the two regimes is also evident in the middle and upper level troposphere (Figures 5c–5f). Under the WR, at 600 hPa, westerlies cover most of South Asia south of the Tibetan Plateau (Figure 5c). Upper level (200 hPa) divergence dominates widely over South Asia reflecting active convection. In contrast, a closed low is observed centered on about 20°N, 85°E under the ER (Figure 5d). The low is detected from the surface up to 400 hPa (figure not shown). Thus, the meridional pressure gradient around the Gangetic Plain is reversed between the WR and ER below the mid-level troposphere. Strong southeasterly/easterly flow appears over the Gangetic Plain along the northern peripheries of the low. The area of high-specific humidity extends around the head of the Bay of Bengal, probably reflecting strong convection over the bay and moisture transport due to the low. Note that, unlike the WR, a synoptic-scale weak upper level divergence with an area of weak convergence around Bangladesh covers the Gangetic Plain where low precipitation is observed (Figure 5f). Also, at 925 hPa there is low-level wind divergence around the Gangetic Plain (figure not shown). The synoptic-scale low under the ER resembles the composite structure of low-pressure systems (LPSs) such as monsoon lows and depressions that initiate over the head of the Bay of Bengal and move northwestward toward India during summer (Godbole, 1977; Hunt et al., 2016; Krishnamurthy & Ajayamohan, 2010). The frequency and tracks of LPSs depend strongly on the phase of the ISOs (Goswami et al., 2003; Krishnamurthy & Ajayamohan, 2010; Hatsuzuka & Fujinami, 2017). Under the ER (i.e., the break phase of the ISO), which generally corresponds to the active phase of the ISO around central India, LPSs typically form over the head of the Bay of Bengal and move northwestward. The LPSs have precipitation maxima (minima) from west (northeast) to south (north) of their center (Hurley & Boos, 2015; Krishnamurthy & Ajayamohan, 2010). Thus, when LPSs are located between the head of the Bay of Bengal and eastern

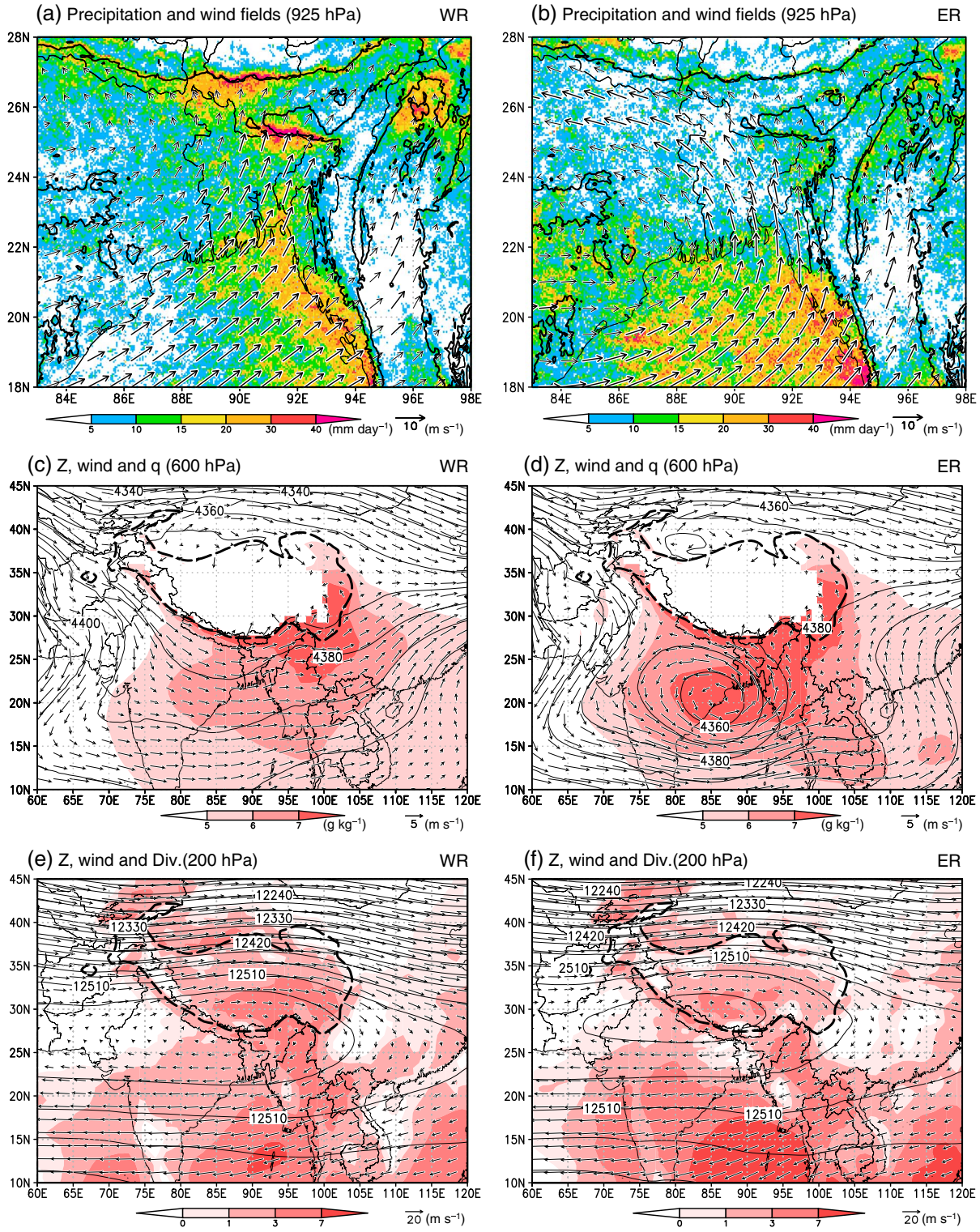


**Figure 5.** (a) Composite of precipitation (shading) and wind fields (vectors) at 925 hPa for the WR. The 500 m topographic contour is indicated by the thick solid line. Wind vectors with speeds greater than (less than) 6 m $s^{-1}$ are drawn as thick (thin) arrows. (b) As in Figure 5a but for the ER. (c) Composites of geopotential height (contours), wind fields (vectors), and specific humidity (shading) at 600 hPa under the WR. The contour interval is 10 gpm. The 3,000 m topographic contour (as used in ERA-Interim) is drawn as the thick dashed line. (d) As in Figure 5c but for the ER. (e) Composite of geopotential height (contours), wind fields (vectors), and wind divergence at 200 hPa (shading) under the WR. The contour interval for geopotential height is 30 gpm. Areas of divergence greater than zero are shaded. The units for divergence are $1.0 \times 10^{-6}$ $s^{-1}$. (f) As in Figure 5e but for the ER. Note that the area covered in Figures 5c–5f is broader than the domain in Figures 5a and 5b.

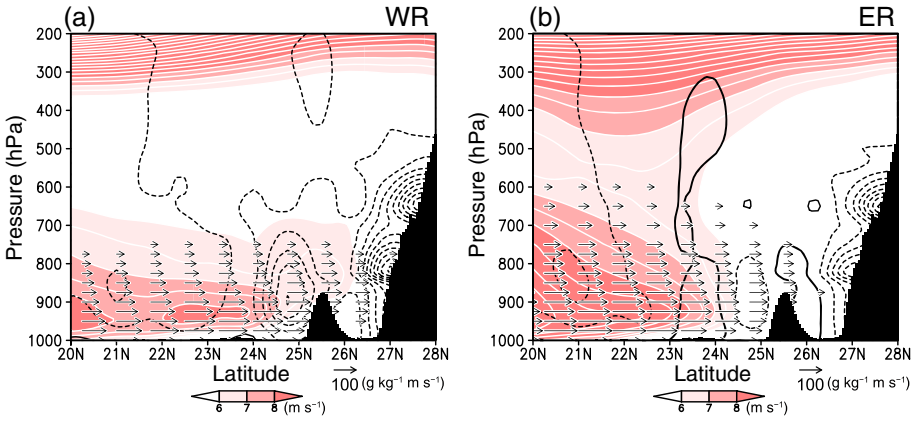


**Figure 6.** (a) Latitude-height cross section of the meridional component of water vapor flux (vectors), horizontal wind speed (shading), and vertical velocity (black contours) averaged between 90.5°E and 92°E under the WR. The contour interval for wind speed is 0.5 m $s^{-1}$. The contour interval for vertical velocity is 0.06 Pa $s^{-1}$; the dashed (solid) black contour indicates upward (downward) flow. Black shading denotes the topography; the peak from 25°N to 26°N is the Meghalaya Plateau. Water vapor flux vectors less than 30 g $kg^{-1}$ m $s^{-1}$ are omitted. A latitude of about 22.5°N corresponds to the coastline. (b) As in Figure 6a but for the ER.

India, precipitation tends to decrease around the Meghalaya Plateau, consistent with our results for the ER.

Figure 6 shows a latitude-height cross section for the horizontal wind speed, meridional component of water vapor flux, and vertical velocity at the longitude of the Meghalaya Plateau. The low-level horizontal jet structure with a core at 925 hPa is common to both regimes. The upper level strong wind above 300 hPa is the easterly jet stream of the southern part of the Tibetan high in the upper level troposphere (Figures 5e and 5f). This low-level and upper level jet structure is a typical feature of the Asian summer monsoon circulation around South Asia. Under the WR, the low-level strong wind (>6 m $s^{-1}$) reaches the southern slopes of the Meghalaya Plateau (Figure 6a). Large water vapor transport toward the southern slope corresponds to the low-level jet below the height of the plateau. A local maximum of upward flow is observed around the southern slope due to forced lifting of moist air. Upward flow extends throughout the area of the cross section, reflecting the active phase of the ISO. Under the ER, strong low-level winds from the Bay of Bengal cannot reach the southern slopes (Figure 6b). Therefore, moisture transport toward the plateau decreases drastically north of 24°N. The stronger wind speeds from 800 hPa to 400 hPa to the south of 23.5°N in the ER comes from a strong pressure gradient due to the low (Figure 5d). There is weak subsidence from the midlevel to low-level troposphere from 23°N to 26°N under the ER, consistent with the area of low-level wind divergence and weak upper level convergence. A weak upward flow is also detected around the southern slope of the plateau.

Equivalent potential temperature ($\theta_e$) profiles show that atmospheric stratification below 600 hPa is slightly more unstable for moist convection under the WR than the ER windward of the southern slopes (Figure 7). The potential temperature profile is nearly identical in the two regimes. $\theta_e$ under the WR is slightly higher below 900 hPa, but lower between 850 and 500 hPa, than under the ER, which is caused by the difference in specific humidity profiles (not shown). The difference in specific humidity in the midlevel troposphere is probably related to the difference in atmospheric circulation around Bangladesh (Figures 5c, 5d, and 6). However, atmospheric stability alone cannot explain the large difference in precipitation over the southern slope between the two regimes, although the vertical $\theta_e$ profile of the WR is more favorable for cumulus-type convection than in the ER. Therefore, identification of the mechanical processes involved in regulating forced lifting over the southern slope is needed. The low-level horizontal wind speed toward the southern plateau can be a major driver (Figure 6a). The synoptic-scale vertical flow can also affect the orographic effect of forced ascent.

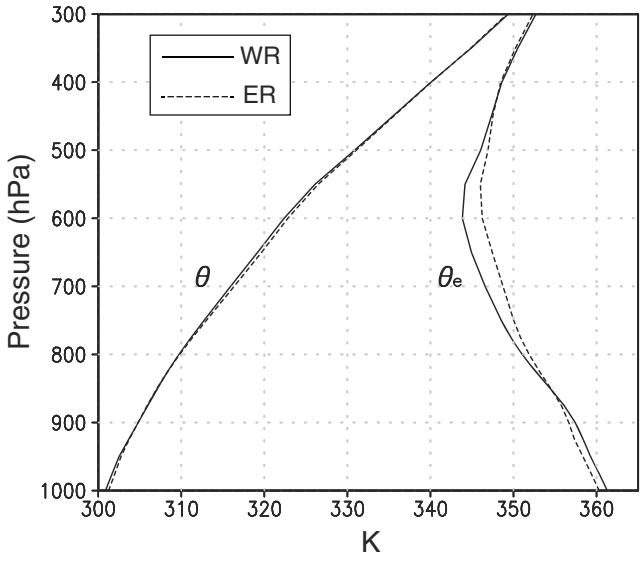


**Figure 7.** Vertical profiles of potential temperature and equivalent potential temperature over the area bounded by 90°–92°E, 24°–25°N south of the Meghalaya Plateau in the WR (solid line) and ER (dashed line).

In short, under the WR, strong low-level winds with jet-like structures that encounter the southern slope of the plateau trigger forced ascent of moist air over the southern slope and then promote condensation and precipitation during the large-scale upward motion around the Gangetic Plain related to the active phase of the ISO. In contrast, in the ER, weak low-level wind toward the southern slope, low-level divergent fields, and subsidence around the Gangetic Plain inhibit forced lifting and condensation, reducing precipitation significantly over the southern slope.

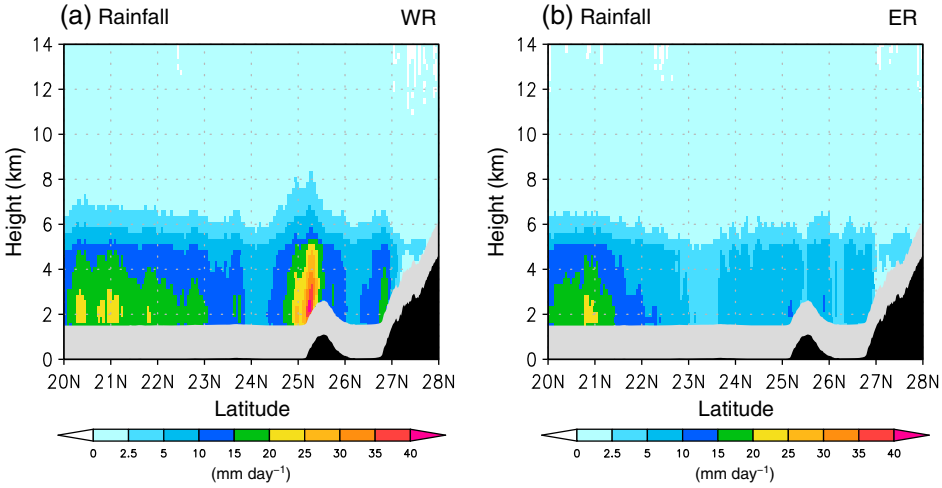


**Figure 8.** (a) Vertical structure of rainfall (mm $d^{-1}$) averaged over 90.5°E to 92°E under the WR. Black shading indicates topography. Values below 1,500 m above ground level are omitted (gray shading) to eliminate effects of surface clutter. A latitude of about 22.5°N corresponds to the coastline. (b) As in Figure 8a but for the ER.

### 3.3. Characteristics of Precipitation

First, we describe some important characteristics of the topography of the Meghalaya Plateau that can affect the precipitation field. The southern margin of the plateau is very steep and rugged, especially from 91° to 92°E, with surface elevation above 1,500 m and steep cliffs and deep narrow valleys facing the plain of Bangladesh (Figure 1b). Cherrapunjee (25.25°N, 91.73°E) is located on the southern part of the plateau near such a deep valley. A relatively flat highland extends along the crest of the plateau at elevations above 1,500 m. The northern periphery, which faces the Brahmaputra Valley, is also steep but less steep than the southern slope and is not as rugged as the southern periphery.

Under the different synoptic conditions of the two regimes, precipitation around the Meghalaya Plateau exhibits remarkable differences. Figure 8 shows the height-latitude cross section of rainfall at the longitude of the Meghalaya Plateau. High rainfall (>40 mm $d^{-1}$) is concentrated over the southern slopes of the Meghalaya Plateau under the WR. The rainfall maximum is observed between 2,000 and 3,000 m above sea level over the southern slopes. Rainfall decreases markedly from the crest to the northern slopes of the plateau. These observations strongly support the role of the southern slopes of the Meghalaya Plateau as an orographic barrier against the strong low-level southwesterly/southerly flow, producing orographic rainfall there via the forced uplift of moist air in the WR (Figure 6a). In contrast, rainfall is clearly low around the Meghalaya Plateau under the ER. Weak rainfall peaks (10–15 mm $d^{-1}$) at 2,000 to 3,000 m above sea level are observed over the southern and northern slopes of the plateau; less rainfall occurs over the crest of the plateau. The areas with precipitation less than 5 mm $d^{-1}$ at 3 km in height correspond well to the areas of subsidence (Figure 6b).

High-resolution TRMM PR data reveal the detailed spatial structure of precipitation around the Meghalaya Plateau under the two regimes (Figure 9). Rainfall of more than 50 mm $d^{-1}$ is concentrated over the rugged southern slopes from 91° to 92°E (Figure 9a) where the steep slope (or cliff) rises to 1,500 m (Figure 1b). Rainfall maxima of more than 60 mm $d^{-1}$ appear in the narrow valleys of the southern slopes from 91° to 92°E. The valley (25.25°N, 91.8°E) immediately to the east of Cherrapunjee has the highest rainfall of 88.4 mm $d^{-1}$. An area of more than 20 mm $d^{-1}$ spreads southward off the southern slopes at 24.5°N. There are two maxima of rainfall frequency from 91° to 91.5°E and from 91.5° to 92°E around the southern slopes (Figure 9b). The area of high rainfall corresponds well to that of high rainfall frequency. However, high rain intensity (>8 mm $h^{-1}$) is narrowly confined over the southern slopes (Figure 9c), indicating that both high rain frequency and intensity contribute to high rainfall (>50 mm $d^{-1}$) over the southern slopes. Between 50% and 70% of the rainfall is convective over the southern slopes, whereas from the crest to the northern slopes, more than 70% of rainfall falls as stratiform rain (almost all rain that is not convective is stratiform). The high convective fraction also spreads to the south of the plateau. In contrast, under the ER, rainfall is nearly the same on the southern and northern slopes (Figure 9e), at around 10–20 mm $d^{-1}$. The top of the plateau enclosed by the 1,500 m contour has low rainfall of less than 5 mm $d^{-1}$. Relatively high rain frequency (10% to 15%) is observed over the southern and northern slopes, whereas in between, on the crest of the plateau, it is less than 10%. Rain intensity seems to be slightly higher on the southern slopes than on the northern slopes. The convective rain fraction over the southern slopes decreases to between 30% and 50%. The spatial distribution of rainfall depends on that of rain frequency around the plateau, as under the WR.

### 3.4. Diurnal Variation of Precipitation

Next, we will examine the diurnal variation of rainfall frequency around the Meghalaya Plateau under the WR and ER because these diurnal variations are essential to our understanding of the high rainfall over the

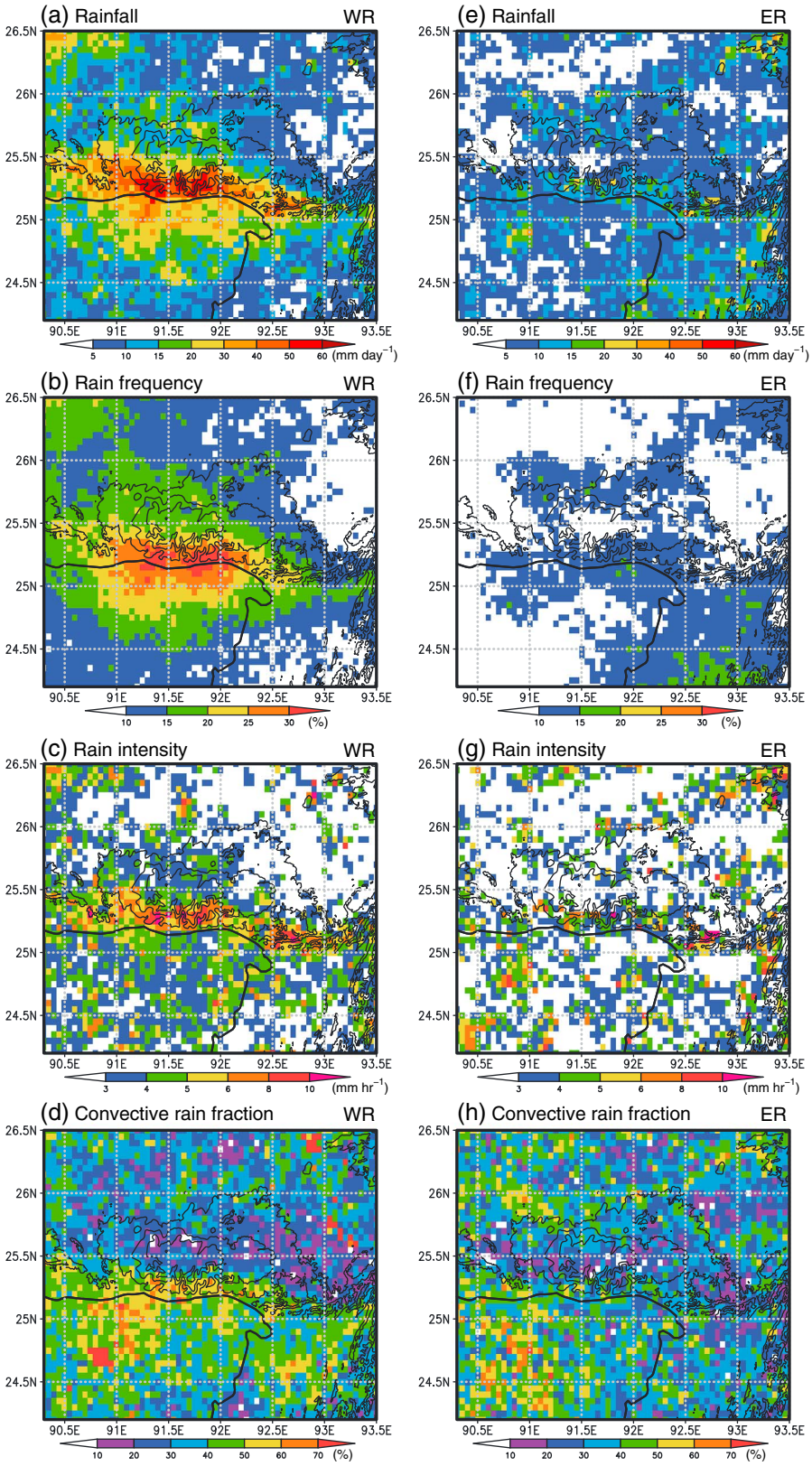


**Figure 9.** Horizontal distribution of (a) rainfall (mm $d^{-1}$), (b) rain frequency (%), (c) rain intensity (mm $h^{-1}$), and (d) convective rain fraction (%) under the WR. Topographic contours for 500, 1,000, and 1,500 m are shown as thin solid lines. (e)–(h) As in Figures 9a–9d but for the ER.

southern slopes under different wind regimes. Hourly gridded rainfall and rain frequency were smoothed with a 3 h running mean to reduce sampling errors. We used the unified local time (LT; UTC + 6 h) along 90°E because the study area was limited to the region around Bangladesh. Figure 10 shows a time-longitude section for rain frequency along the southern slopes of the plateau. Under both regimes, a maximum rain frequency appears from 0000 to 0600 LT. Overall, rain frequency is higher under the WR than the ER at the same LT over the southern slopes. Under the WR, rainfall tends to occur frequently throughout the day but shows a diurnal variation. High rain frequency (>24%) starts about 2100 LT in the area between 91° and 92.5°E. The rain frequency then reaches its maximum (>42%) from 0000 to 0300 LT. There appear to be two maxima, from 0000 to 0300 LT and 0600 to 0900 LT, on the slopes around 91° to 91.5°E. The southern slopes around 91.6° to 92.2°E, where the grid cell with highest rainfall is located in a narrow valley next to Cherrapunjee, exhibit a continuous high rain frequency (>18%) throughout the day and with a diurnal variation. In contrast, under the ER, a very low rain frequency (<6%) is observed from 0900 to 1800 LT. After 1800 LT, rain frequency increases gradually and reaches its maximum from 0000 to 0300 LT (>24% around 92°E). Rainfall frequency is high (>24%) in the area between 91.5° and 92.5°E.

To highlight the contrast between the northern slopes (25.2°–25.4°N), the southern slopes (25.7°–25.9°N), and the area south of the plateau, Figure 11 shows the diurnal variation of rainfall over the northern and southern slopes of the plateau, and the time-latitude section showing rain frequency over the longitude range of the plateau. The general features of the diurnal variation of rain frequency along the southern slopes (Figure 11) are as in Figure 10. In correspondence with the rainfall frequency along the southern slopes, rainfall increases from 2100 LT and reaches more than 3 mm $h^{-1}$ during the period 0000–0300 LT over the southern slopes

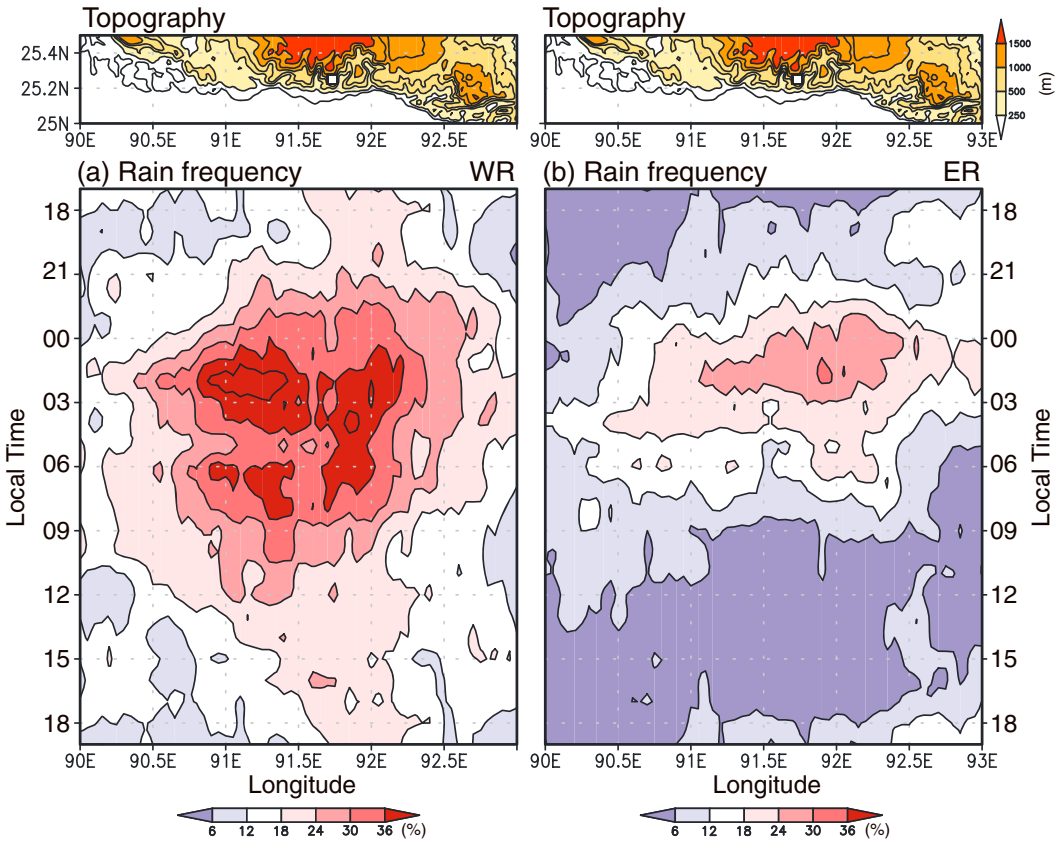


**Figure 10.** (a) Longitude-time (LT at 90°E) section of rain frequency averaged between 25.2°N and 25.4°N under the WR. (b) As in Figure 10a but for the ER. The contour interval is 6%. Relevant topography is shown above each panel. The white square on the southern slopes of the plateau indicates the location of Cherrapunjee station (25.25°N, 91.73°E).

(Figure 11a), and rainfall of approximately 2 mm $h^{-1}$ continues to 1200 LT. A minimum value of less than 1 mm $h^{-1}$ is observed from 1200 to 1800 LT. In contrast, on the northern slopes, rain frequency increases from 0000 LT and relatively high values (>12%) continue until 1200 LT (Figure 11d). The maximum rain frequency then develops from 1200 to 1500 LT, and rainfall reaches more than 1 mm $h^{-1}$ over this period (Figure 11a). Almost simultaneously, rain frequency also increases over the plain from 23° to 25°N and reaches its maximum between 1200 and 1500 LT. The area between 23.5° and 24.5°N (northeastern Bangladesh) has two maxima (0000–0600 and 1200–1500 LT), which is consistent with the findings of Terao et al. (2006). Rainfall frequency is at a minimum during the period 1800–2100 LT from 20° to 26.5°N. Under the ER, relatively high rain frequency (>18%) appears only from 0000 to 0600 LT over the southern slopes, whereas rainfall is frequent (>18%) from 1200 to 1800 LT over the northern slopes. The diurnal variation in rainfall is consistent with that in rainfall frequency (Figure 11b). The maximum values of rainfall are about 1 mm $h^{-1}$ on the northern and southern slopes. Rain frequency remains low on the crest of the plateau all day. Thus, the local maxima in rainfall and rain frequency over both the northern and southern slopes under the ER, seen in Figures 8b, 9e, and 9f, represent rainfall with different peak phases of diurnal variation. Low rain frequency is observed over the plain from 22.5° to 24°N throughout the day, resulting in low rainfall there (Figure 5b). The diurnal variation with larger amplitude results in larger daily total rainfall around the plateau under both regimes, although the minimum value of rainfall during daytime in WR is also larger than that in ER.

### 3.5. Diurnal Variation of Low-Level Wind Fields

In this subsection, we examine the diurnal variation of low-level wind over the area windward of the plateau (i.e., Bangladesh) to improve our understanding of the nocturnal enhancement of rainfall. Figure 12 is a height-latitude cross section of the difference in the meridional wind component and horizontal wind

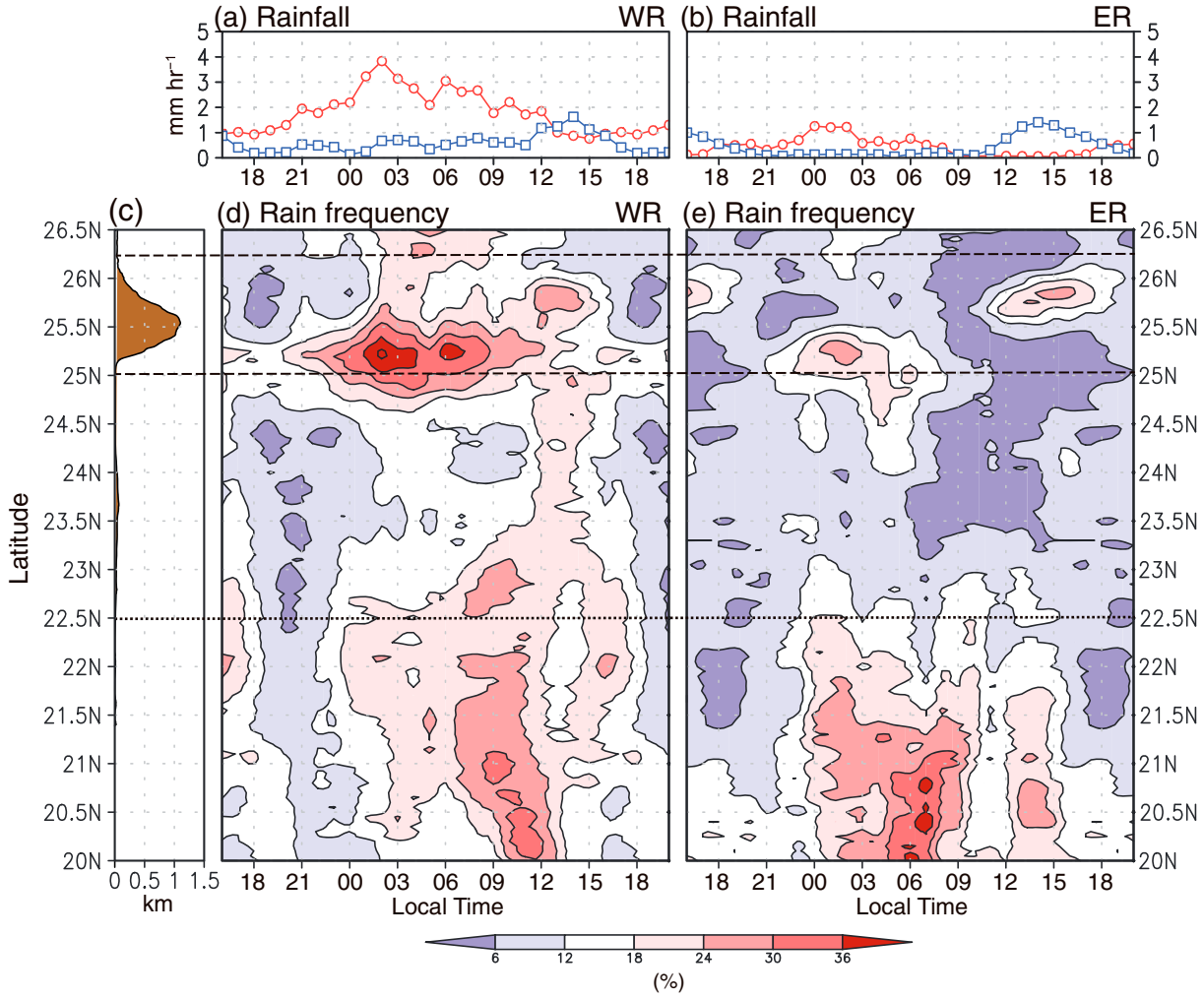


**Figure 11.** (a) Diurnal variation of rainfall (mm $h^{-1}$) over the southern (25.2°–25.4°N, 90.5°–92°E; red solid line with open circles) and northern slopes (25.7°–25.9°N, 90.5°–92°E; blue solid line with open squares) of the Meghalaya Plateau under the WR. (b) As in Figure 11a but for the ER. (c) Surface elevation averaged between 90.5° and 92°E. (d) Latitude-time (LT at 90°E) section of rain frequency averaged between 90.5° and 92°E. The two dashed lines at 25°N and 26.25°N denote the southern and northern edges of the Meghalaya Plateau, respectively. The dotted line at 22.5°N corresponds approximately to the Bangladesh coastline along the Bay of Bengal. (e) As in Figure 11d but for the ER.

speed between 0000 and 1200 LT, which corresponds to the time of maximum rainfall frequency and the beginning of the period of minimum rain frequency (Figures 10 and 11). It is worth noting that northward wind speed below 850 hPa is higher at midnight than at noon over the Bangladesh lowlands under both regimes, suggesting an enhancement of low-level moisture transport toward the southern slope and orographically forced lifting during the night (Figure 6). The maximum difference in horizontal wind (>2 m $s^{-1}$) appears at 950 hPa centered around 24°N.

Figure 13 presents composites of wind fields at 950 hPa at 1200 and 0000 LT under the two regimes to show the overall spatial distribution of wind fields from the Bay of Bengal to the plain of Bangladesh. Under the WR, it is worth noting that an area of stronger wind extends north-south on the windward side of the Arakan Mountains from 22° to 25°N, blowing parallel to the mountains and toward the plateau (Figure 13a). The strong winds strengthen further at 0000 LT (Figure 13b). At 0000 LT, under the WR (Figure 13b), overall, the strong wind from the Bay of Bengal can intrude into the plain up to 25°N without significant reduction of wind speed, while a notable decrease occurs over land at 1200 LT as the southwesterly flow moves inland (Figure 13a). Under the ER, the southerlies/southeasterlies are enhanced along the Gangetic Plain as a whole during the night. There is a north-south area of strong winds parallel

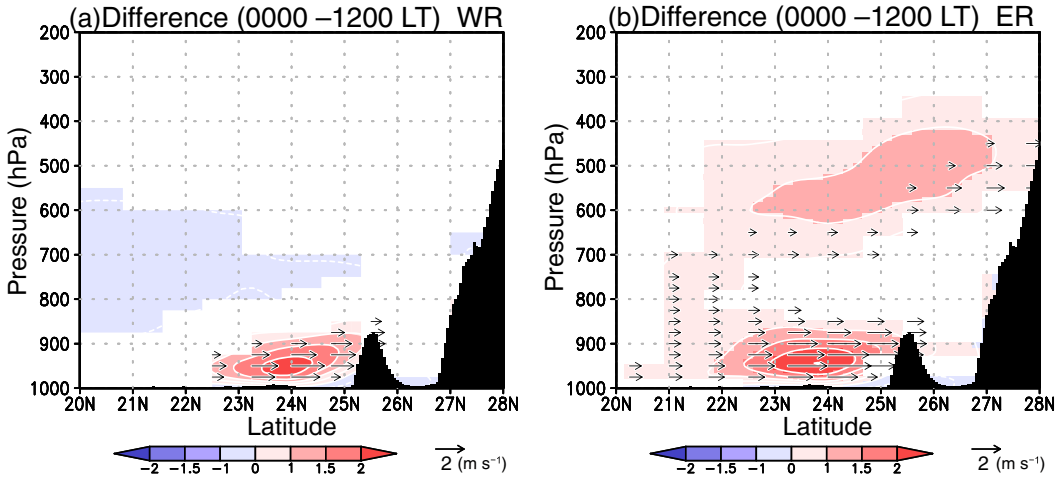


**Figure 12.** (a) Latitude-height cross section of the difference in the meridional wind component (vectors) and horizontal wind speed (shading) between 0000 and 1200 LT under the WR. Only differences in wind speed that are statistically significant at the 99% level are plotted. The differences in meridional wind vectors with speeds less than 0.5 m $s^{-1}$ are omitted. The values are averaged between 90.5°E and 92°E. Black shading indicates topography. The latitude of about 22.5°N corresponds to the coastline. (b) As in Figure 12a but for the ER.

to the Arakan Mountains between 20° and 23°N, which is shifted southward compared to that in the WR, probably due to the synoptic-scale pressure gradient and the topography (Figure 5). The enhancement of the southerly component toward the southern slopes of the plateau is evident at 0000 LT south of the plateau.

Under the WR, the speed of southerlies/southwesterlies at 950 hPa upwind of the plateau over Bangladesh is higher at 0000 and 0600 LT than the daily mean value but lower at 1200 LT (not shown). The winds at 1800 LT are almost the same as the daily mean. In contrast, under the ER, southerly components stronger than the daily mean are only observed at 0000 LT. As under the WR, the wind speed is lower than the daily mean at 1200 LT. The wind fields at 0600 and 1800 LT are nearly equal to the daily mean fields. These results support the persistent (2100–1200 LT) high rainfall frequency under the WR and the relatively shorter period (0000–0600 LT) of modest rainfall frequency under the ER.

## 4. Discussion

### 4.1. Low-Level Jets

Under the WR, the localized strong southerly flow that extends north-south parallel to the Arakan Mountains and toward the Meghalaya Plateau (Figures 13a and 13b) is an important characteristic of the wind field in the low-level troposphere, as are the strong southwesterlies over Bangladesh as a whole. The vertical structure of wind speed around Bangladesh reveals a clear low-level jet (LLJ) structure along the western side of the Arakan Mountains (Figures 14a and 14b). At 0000 LT, the core of maximum wind speed is located at 950–925 hPa from 91° to 92°E, and the area of strong wind extends upward along the western slopes of the Arakan Mountains and below the height of the mountains (Figure 14b). The LLJ parallel to the Arakan Mountains has the characteristics of a barrier jet, which is a mountain-parallel wind maximum resulting from geostrophic adjustment as stable nocturnal air is advected against an elongated topographic ridge (Parish, 1982; Li & Chen, 1998; Houze, 2012). Actually, the wind velocities satisfy the thermal wind balance (Figure 14b). The southerly LLJ is further enhanced during the nighttime relative to that in the daytime (Figures 13b and 14b).

The nocturnal acceleration and daytime deceleration of the LLJ are related to the diurnal variation of the atmospheric boundary layer over land. Figure 14c shows the height-latitude cross section of potential temperature and horizontal wind speed at 1200 LT for the longitude range of the Meghalaya Plateau under

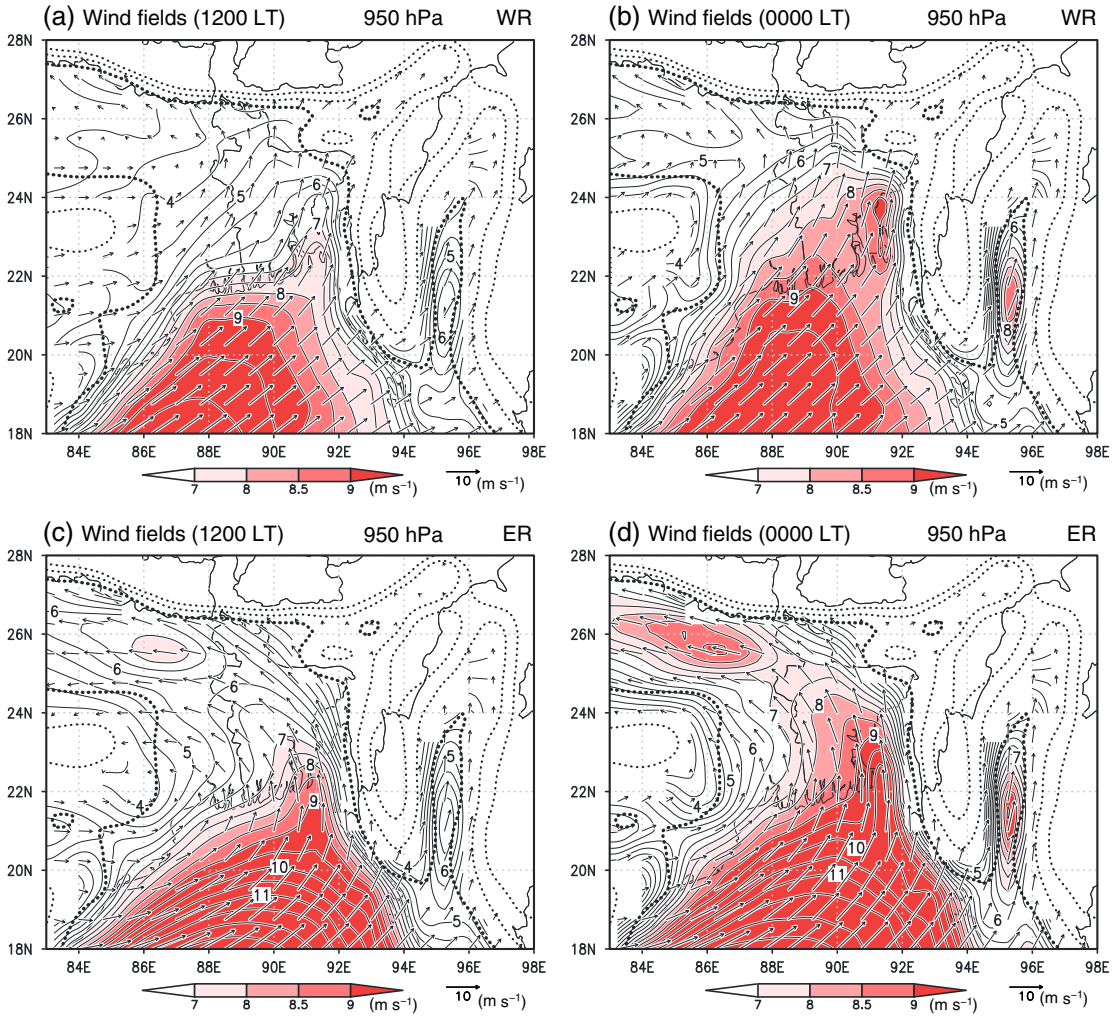


**Figure 13.** (a) Composites of horizontal wind (vectors) and wind speed (contours) at 950 hPa at 1200 LT under the WR. The contour interval for wind speed is 0.5 m $s^{-1}$. Areas of wind speed greater than 7 m $s^{-1}$ are shaded. The topographic contours for 250 (500 and 750) m are drawn as thick (thin) dotted lines. The topographic data are from the ERA-Interim reanalysis. (b) As in Figure 13a but for 0000 LT. (c, d) As in Figures 13a and 13b), but for the ER.

the WR. A vertically well-mixed layer is observed from 23° to 24°N below 950 hPa (~ 500 m above sea level), which is the level of the maximum amplitude of diurnal variation in horizontal wind (Figure 12a), that is caused by sensible heat flux from the surface during daytime. Note that a maximum of rainfall frequency appears from 1200 to 1500 LT over the plain under the WR, which is indicative of active moist convection caused by the surface heating. The lifting condensation level (LCL) of the air at the surface is about 500 m above sea level at 1200 LT, which corresponds approximately to the 950 hPa level. Potential temperature can become vertically homogeneous due to active dry convection below the LCL (i.e., subcloud layer). The vertically well-mixed layer reduces horizontal wind speed because the vertical mixing within the mixed layer acts as a frictional force on the horizontal wind. Therefore, the LLJ is weakened over land. The wind maximum appears to rise from 925 hPa at 20°N to 900 hPa at 24°N as the wind moves over land (Figure 14c), and the zonal section (Figure 14a) shows that the core of wind speed is centered at 900 hPa at 1200 LT. In contrast, surface cooling after sunset generates a stable surface layer during the night (Figures 14b and 14d), and the atmospheric boundary layer decouples from the atmosphere above. Therefore, the speed of the LLJ increases, particularly around 950–925 hPa, because the strong low-level southeasterly wind from the Bay of Bengal can flow over the flat lowland without being slowed down greatly by surface friction. The inertial oscillation can also enhance the nocturnal LLJ (Blackadar, 1957; Rife et al., 2010; Van de Wiel et al., 2010; Ruchith et al., 2014). The acceleration of the jet occurs above the neutrally stratified layer above 950 hPa. This

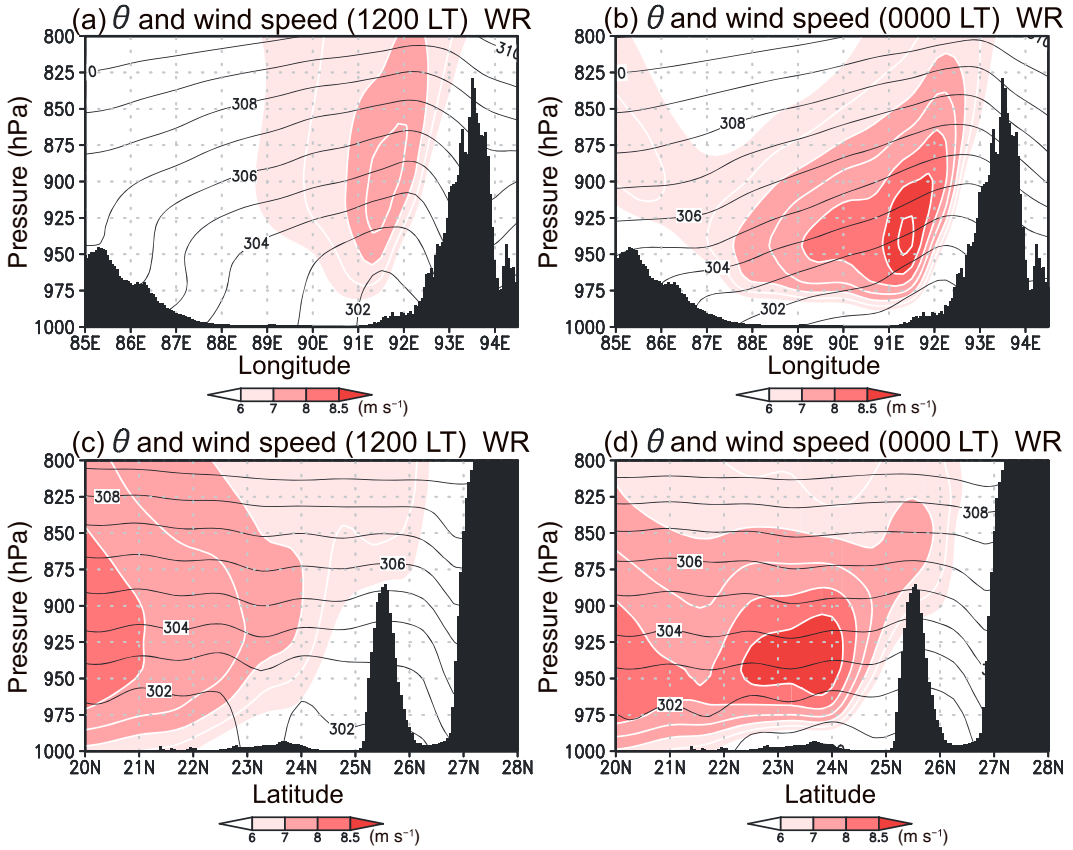


**Figure 14.** (a) Longitude-height cross section of potential temperature (black contours) and horizontal wind speed (shading) averaged between 22°N and 24°N at 1200 LT under the WR. The contour interval for potential temperature is 1 K. The contour interval for horizontal wind speed is 0.5 m $s^{-1}$ (white contours). Black shading indicates topography. The topography from 92° to 94°E corresponds to the Arakan Mountains. (b) As in Figure 14a, but for 0000 LT. (c and d) As in Figures 14a and 14b but for a latitude-height cross section averaged between 90.5°E and 92°E. The latitude of about 22.5°N corresponds to the Bangladesh coastline along the Bay of Bengal.

might be due to moist convection during the afternoon as discussed in Terao et al. (2006). The height variations in the LLJ from daytime to nighttime might also play an important role in regulating the level from which moist air is frequently raised upward by the southern slopes of the Meghalaya Plateau. Thus, the barrier jet along the coastal mountains (e.g., the Arakan Mountains) and its diurnal variation create environment that concentrates moist strong wind onto the southern slopes and enhances local precipitation. Based on the present results and discussion, a schematic of the mechanism of diurnal variation of the LLJ in the WR is presented in Figure 15.

Under the ER, the wind speed difference between midnight and noon is greater than that under the WR south of the plateau (Figure 12b). The height of the mixed layer is higher under the ER (~925 hPa) than under the WR (~950 hPa; figure not shown). The surface energy budget balances the net radiation against the sensible heat flux, latent heat flux, and ground heat flux. Soil moisture alters the partitioning of energy between the surface energy budget components (i.e., sensible heat flux and latent heat flux) significantly. Sensible heat flux becomes larger than latent heat flux over drier ground surfaces (see e.g., Tanaka et al., 2007). In addition, the incoming solar radiation is likely larger in the ER than the WR because of suppressed moist convection over Bangladesh during daytime under the ER (Figure 11e). Thus, the larger incoming solar radiation and drier ground surface during daytime can shift the mixed layer higher under the ER. A higher mixed-layer top suggests the existence of more active vertical mixing by dry convection, indicating the layer may act as a stronger frictional force on the horizontal wind. Thus, the higher mixed layer could lead to larger diurnal wind differences.

We note that the nocturnal acceleration of the low-level wind over the land is the opposite of the land-sea breeze circulation in which the low-level onshore wind is strengthened during the daytime. The nocturnal

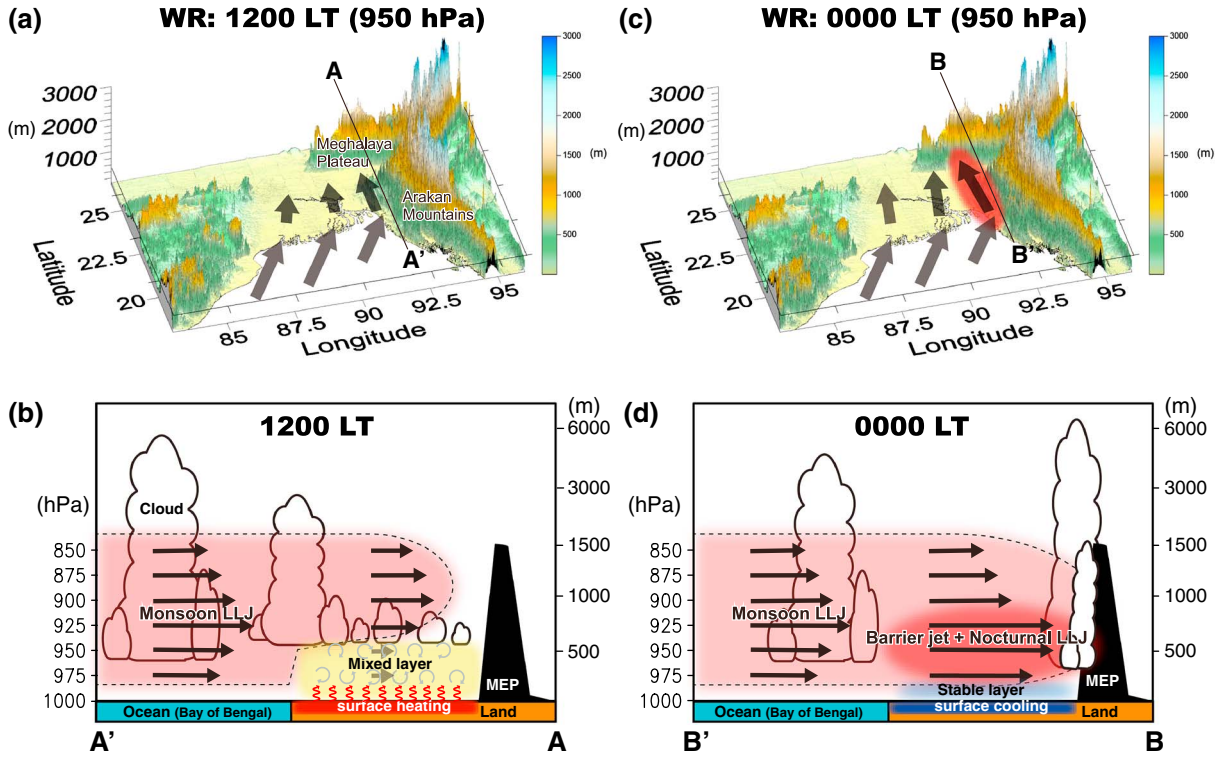


**Figure 15.** Schematics of diurnal variation in the low-level jet (LLJ) and atmospheric boundary layer from the Bay of Bengal to the Meghalaya Plateau (MEP) under the WR. (a) Representative horizontal wind at 950 hPa over the ocean and land at 1200 LT with 3-D topography. The vector length is proportional to the wind speed. (b) Vertical section along the line A–A′ in Figure 15a. Arrows over the ocean and land indicate representative horizontal wind speeds in the two regions at pressure levels in the lower troposphere that represent the vertical profile of the LLJ toward the Meghalaya Plateau. Shading enclosed by the dotted line indicates the envelope of the monsoon LLJ. (c) As in Figure 15a but for 0000 LT. The elliptical area parallel to the Arakan Mountain indicates a strong LLJ due to the barrier jet and nocturnal jet that cause the nocturnal rainfall over the southern slope of the plateau. (d) As in Figure 15b but for 0000 LT along the line B–B′ in Figure 15c.

enhancement of the horizontal onshore wind from the ocean is a common feature over lowlands facing the ocean, such as those in Bangladesh, northeastern India, northwestern India, Myanmar, and the Indochina Peninsula in South/Southeast Asia (Figure 16).

### 4.2. Comparison With the Himalayas

Here we discuss the properties of precipitation on the Meghalaya Plateau based on a comparison with the Himalayas, as these two regions have some common features, such as having southern slopes facing the Gangetic Plain and a nocturnal maximum of rainfall over the southern slopes, although their vertical and spatial scales are quite different. Using the TRMM PR, previous studies showed two distinct zonally elongated rainfall peaks appear over the southern slopes of the central Himalayas in Nepal during summer associated with the parallel ranges (i.e., the Lesser Himalayas and sub-Himalayas) (Bookhagen & Burbank, 2006; Shrestha et al., 2012). The active and break phases in the central Himalayas correspond approximately to the WR and ER in this study (Figures 5a and 5b). The two rainfall peaks of the central Himalayas are primarily determined by the high rain frequency (Shrestha et al., 2012). The rain intensity along the slope, however, shows a monotonic decrease with elevation regardless of the major relief of the Himalayas. In addition, the value of the rain intensity is nearly the same in both active and break phases in the central Himalayas.

In contrast, on the southern slopes of the Meghalaya Plateau in the WR, both high rain frequency and high rain intensity determine the high rainfall peak (Figures 9a–9c). In the ER, both rain frequency and rain intensity show a marked decline around the plateau, resulting in low precipitation (Figures 9e–9g). The primary cause of the difference in rain intensity in the active and break phases between the two areas may be the difference in wind speed of the low-level wind that blows normal to the slopes. The strong and moist low-level southerlies from the Bay of Bengal can reach the Meghalaya Plateau easily because of the topography

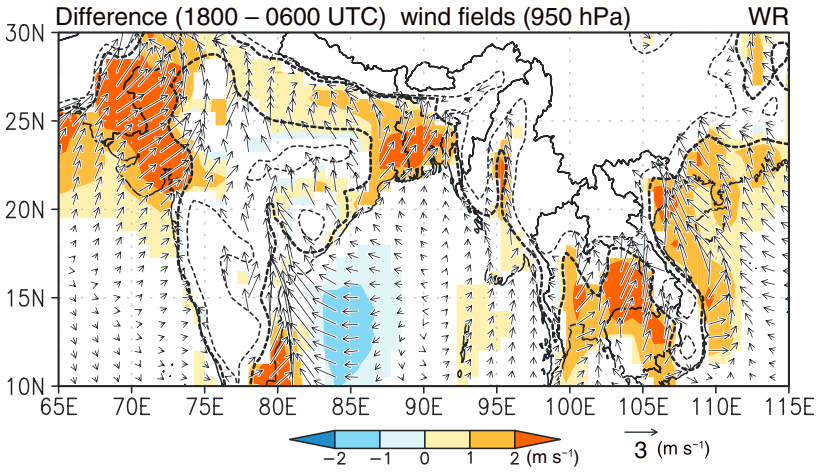


**Figure 16.** Composite difference of horizontal wind (vectors) and wind speed (shading) at 950 hPa between 1800 and 0600 UTC (0000 and 1200 LT, respectively, at 90°E) in the WR. Only differences in wind speed that are statistically significant at the 99% level are shaded. Thick (thin) dashed lines show the 250 (500) m topographic contours from the ERA-Interim reanalysis.

(Figure 1a), while in the central Himalayas the Chota Nagpur Plateau and the Deccan Plateau block the low-level strong southwesterlies from the Bay of Bengal.

As for the Meghalaya Plateau, the Himalayas in Bhutan receive high rainfall under the WR (Figure 5a). The low-level southerlies can reach the southern slopes of the Himalayas in Bhutan through the lowland between the Meghalaya Plateau and the Chota Nagpur Plateau. Forced uplift occurs readily, resulting in precipitation with high intensity and high frequency (figure not shown). Thus, precipitation features in the Himalayas seem to be different between Nepal and Bhutan. In addition, the low-level southerlies toward Bhutan are also enhanced at 0000 LT (Figure 13b), resulting in a nocturnal rainfall maximum, as on the Meghalaya Plateau (figure not shown). The results suggest that the prevailing wind over the Gangetic Plain, such as the WR and ER, and nocturnal LLJ, significantly affects precipitation features including the diurnal variation over the Himalayas around Bhutan. Further studies are needed to understand how the interaction between diurnally varying LLJ over the Gangetic Plain and the mountain-valley wind system along the southern slopes affects the diurnal variation of precipitation over the slopes in both the Meghalaya Plateau and the Himalayas.

## 5. Summary

Seventeen years of TRMM PR data have revealed the fine spatial distribution of precipitation features during the boreal summer on the Meghalaya Plateau, one of the wettest places in the world. In summer, strong low-level monsoon southwesterlies with the properties of a low-level jet (LLJ) over the Bay of Bengal blow into the plains of Bangladesh. The Meghalaya Plateau is located at the far northeastern edge of the plain and is the first regional-scale orographic barrier (<2,000 m) against the low-level onshore wind. Moist and strong low-level wind is a major driver of orographic precipitation. Therefore, we focused on the low-level wind direction to investigate precipitation features in different convective regimes around the plateau.

According to statistical analysis, precipitation around the plateau fell into two distinct regimes based on the low-level wind direction: a westerly regime (WR) and an easterly regime (ER) over Bangladesh that are characterized by high and low precipitation over the southern slopes of the plateau, respectively. The two wind regimes show a contrasting synoptic-scale atmospheric environment throughout the troposphere, including the lower troposphere, around the Gangetic Plain.

Under the WR, strong and moist low-level southwesterly/southerly winds encounter the southern slope of the plateau. Atmospheric stratification over Bangladesh, windward of the plateau, in the lower troposphere is more unstable in regard to moist convection compared with the ER. In addition, large-scale upward flow and upper level wind divergence exist around the Gangetic Plain related to the active phase of the ISO. The synoptic conditions help to promote high orographic precipitation with high rainfall frequency (>30%), high rainfall intensity (>10 mm $h^{-1}$), and high convective rain fraction (>50%) along the southern slopes, probably due to frequent and intense forced ascent, resulting in intense local precipitation (>50 mm $d^{-1}$). Rainfall maxima of more than 60 mm $d^{-1}$ appear in the narrow deep valleys of the southern slopes from 91° to 92°E. Rainfall decreases significantly from the crest to the northern slopes of the plateau where stratiform rainfall dominates (>70%).

In contrast, under the ER, a strong southeasterly wind blows along the Gangetic Plain through northwestern Bangladesh, avoiding the plateau. The southeasterly wind is observed from the surface up to the middle troposphere due to the large pressure gradient of the closed low centered over East India. There are divergent wind fields along the low-level southeasterly flow and weak upper level convergence around

the Gangetic Plain, resulting in weak subsidence below the middle troposphere. The ER environment causes low rainfall frequency (<15%) and intensity (<5 mm $h^{-1}$) along the southern slopes inhibiting frequent and intense forced lifting, thus resulting in low local precipitation. The northern slopes experience nearly the same rainfall and rain frequency as the southern slopes. Precipitation is very low on the crest of the plateau.

Both regimes show diurnal variations in precipitation over the Meghalaya Plateau. Under the WR, high rainfall frequency (24% to 40%) persists from 2100 to 1200 LT the next day, with maxima of rainfall frequency (40%) and rainfall (~ 4 mm $h^{-1}$) during the period 0000–0300 LT. On the northern slopes, rainfall frequency reaches a maximum (24%) between 1200 and 1500 LT. Under the ER, rain frequency is very low (<6%) from 1200 to 1800 LT on the southern slopes. After 1800 LT, rain frequency increases gradually and reaches a maximum (24%) from 0000 to 0300 LT accompanied by precipitation of about 1 mm $h^{-1}$. The northern slopes have low rainfall frequency over the period 2100–0900 LT (<12%) and high rainfall frequency (24%) from 1200 to 1800 LT.

The atmospheric boundary layer processes over the plain of Bangladesh change the structure of the LLJ toward the plateau and cause the diurnal variation under both regimes. The vertically well-mixed layer over land decelerates the prevailing low-level wind toward the plateau at 1200 LT and breaks up the LLJ structure, resulting in the daytime minimum of rainfall over the southern slope. In contrast, the wind speed toward the southern slopes accelerates at 0000 LT and has a clear LLJ structure from 950 to 925 hPa above the surface stable layer. Under the WR environment, the nocturnal southwesterly LLJ over Bangladesh and the localized stronger southerly LLJ parallel to the Arakan Mountains (i.e., the barrier jet) help to concentrate the moisture along the southern slopes, resulting in the nocturnal maximum of high rainfall. In contrast, under the ER with the weak subsidence around the plateau, the nocturnal LLJ enhances the southerly component of the prevailing southeasterlies and encounters the southern slope between 0000 and 0600 LT, providing modest rainfall frequency there.

The detailed precipitation process directly over the slopes of the plateau cannot be investigated using only the reanalysis data. Further numerical studies using cloud-resolving models are required if we are to examine the detailed processes of precipitation around the plateau and the development process of the mixed layer and the associated LLJ structure over Bangladesh under the two different wind regimes. Further studies using observational instruments that can operate continuously and with a high vertical resolution, such as Doppler wind lidar, are needed to better understand how boundary layer (or subcloud layer) development changes the structure of the monsoonal LLJ over the low plains.

**Acknowledgments**

We thank J. Matsumoto, T. Hayashi, T. Terao, H. Masunaga, T. Shinoda, T. Hiyama, and M. Hirose for their helpful discussions. We also thank the anonymous reviewers for helping us to improve the manuscript. This study was conducted with support from the Japan Society for the Promotion of Science (JSPS) KAKENHI Grant JP 26220202, JP 26400465 and JP 15H05464. Portions of this study were conducted as part of a collaborative research program of the Institute for Space-Earth Environmental Research, Nagoya University. The TRMM PR data used in this study were provided by Japan Aerospace Exploration Agency (JAXA) (https://www.gportal.jaxa.jp/gp/top.html). The European Centre for Medium-Range Weather Forecasts (ECMWF) is acknowledged for providing the ERA-Interim reanalysis data (http://apps.ecmwf.int/datasets/). GTOPO30 data are available from the US. Geological Survey (https://lta.cr.usgs.gov/GTOPO30).

## References

Annamalai, H., & Slingo, J. M. (2001). Active/break cycles: Diagnosis of the intraseasonal variability of the Asian summer monsoon. *Climate Dynamics*, *18*, 85–102.

Barros, A. P., Kim, G., Williams, E., & Nesbitt, S. W. (2004). Probing orographic controls in the Himalayas during the monsoon using satellite imagery. *Natural Hazards and Earth System Sciences*, *4*, 29–51.

Bhatt, B. C., & Nakamura, K. (2006). A climatological-dynamical analysis associated with precipitation around the southern part of the Himalayas. *Journal of Geophysical Research*, *111*, D02115. https://doi.org/10.1029/2005JD006197

Biasutti, M., Yuter, S. E., Burleyson, C. D., & Sobel, A. H. (2012). Very high resolution rainfall patterns measured by TRMM precipitation radar: Seasonal and diurnal cycles. *Climate Dynamics*, *39*, 239–258. https://doi.org/10.1007/s00382-011-1146-6

Blackadar, A. K. (1957). Boundary layer wind maxima and their significance for the growth of nocturnal inversions. *Bulletin of the American Meteorological Society*, *38*, 283–290.

Bookhagen, B., & Burbank, D. W. (2006). Topography, relief, and TRMM-derived rainfall variations along the Himalaya. *Geophysical Research Letters*, *33*, L08405. https://doi.org/10.1029/2006GL026037

Chen, T. C., & Chen, J. M. (1993). The 10–20-day mode of the 1979 Indian monsoon: Its relation with the time-variation of monsoon rainfall. *Monthly Weather Review*, *121*, 2465–2482.

Dee, D. P., Uppala, S. M., Simmons, A. J., Berrisford, P., Poli, P., Kobayashi, S., … Vitart, F. (2011). The ERA-Interim reanalysis: Configuration and performance of the data assimilation system. *Quarterly Journal of the Royal Meteorological Society*, *137*, 553–597. https://doi.org/10.1002/Qj.828

Fujinami, H., & Yasunari, T. (2001). The seasonal and intraseasonal variability of diurnal cloud activity over the Tibetan Plateau. *Journal of the Meteorological Society of Japan*, *79*, 1207–1227.

Fujinami, H., Nomura, S., & Yasunari, T. (2005). Characteristics of diurnal variations in convection and precipitation over the southern Tibetan Plateau during summer. *SOLA*, *1*, 49–52. https://doi.org/10.2151/sola.2005-014

Fujinami, H., Hatsuzuka, D., Yasunari, T., Hayashi, T., Terao, T., Murata, F. … Habib, A. (2011). Characteristic intraseasonal oscillation of rainfall and its effect on interannual variability over Bangladesh during boreal summer. *International Journal of Climatology*, *31*, 1192–1204. https://doi.org/10.1002/joc.2146

Fujinami, H., Yasunari, T., & Morimoto, A. (2014). Dynamics of distinct intraseasonal oscillation in summer monsoon rainfall over the Meghalaya–Bangladesh–western Myanmar region: Covariability between the tropics and mid-latitudes. *Climate Dynamics*, *43*, 2147–2166. https://doi.org/10.1007/s00382-013-2040-1

Godbole, R. V. (1977). The composite structure of the monsoon depression. *Tellus*, *29*, 25–40. https://doi.org/10.1111/j.2153-3490.1977.tb00706.x

Goswami, B. N., & Mohan, R. S. A. (2001). Intraseasonal oscillations and interannual variability of the Indian summer monsoon. *Journal of Hydrometeorology*, *14*, 1180–1198.

Goswami, B. N., Ajayamohan, R. S., Xavier, P. K., & Sengupta, D. (2003). Clustering of synoptic activity by Indian summer monsoon intraseasonal oscillations. *Geophysical Research Letters*, *30*(8), 1431. https://doi.org/10.1029/2002GL016734

Hatsuzuka, D., & Fujinami, H. (2017). Effects of the South Asian monsoon intraseasonal modes on genesis of low pressure systems over Bangladesh. *Journal of Climate*, *30*, 2481–2499. https://doi.org/10.1175/jcli-d-16-0360.1

Hatsuzuka, D., Yasunari, T., & Fujinami, H. (2014). Characteristics of low pressure systems associated with intraseasonal oscillation of rainfall over Bangladesh during boreal summer. *Monthly Weather Review*, *142*, 4758–4774. https://doi.org/10.1175/MWR-D-13-00307.1

Hirose, M., & Nakamura, K. (2005). Spatial and diurnal variation of precipitation systems over Asia observed by the TRMM precipitation radar. *Journal of Geophysical Research*, *110*, D05106. https://doi.org/10.1029/2004JD004815

Hirose, M., Oki, R., Shimizu, S., Kachi, M., & Higashiuwatoko, T. (2008). Finescale diurnal rainfall statistics refined from eight years of TRMM PR data. *Journal of Applied Meteorology and Climatology*, *47*, 544–561. https://doi.org/10.1175/2007jamc1559.1

Houze, R. A. (2012). Orographic effects on precipitating clouds. *Reviews of Geophysics*, *50*, RG1001. https://doi.org/10.1029/2011RG000365

Hunt, K. M. R., Turner, A. G., Inness, P. M., Parker, D. E., & Levine, R. C. (2016). On the structure and dynamics of Indian monsoon depressions. *Monthly Weather Review*, *144*, 3391–3416. https://doi.org/10.1175/MWR-D-15-0138.1

Hurley, J. V., & Boos, W. R. (2015). A global climatology of monsoon low-pressure systems. *Quarterly Journal of the Royal Meteorological Society*, *141*, 1049–1064. https://doi.org/10.1002/qj.2447

Iguchi, T., Kozu, T., Meneghini, R., Awaka, J., & Okamoto, K. (2000). Rain-profiling algorithm for the TRMM precipitation radar. *Journal of Applied Meteorology*, *39*, 2038–2052.

Kataoka, A., & Satomura, T. (2005). Numerical simulation on the diurnal variation of precipitation over northeastern Bangladesh: A case study of an active period 14–21 June 1995. *SOLA*, *1*, 205–208.

Kikuchi, K., & Wang, B. (2010). Formation of tropical cyclones in the northern Indian Ocean associated with two types of tropical intraseasonal oscillation modes. *Journal of the Meteorological Society of Japan*, *88*, 475–496. https://doi.org/10.2151/jmsj.2010-313

Kiladis, G. N., Wheeler, M. C., Haertel, P. T., Straub, K. H., & Roundy, P. E. (2009). Convectively coupled equatorial waves. *Reviews of Geophysics*, *47*, RG2003. https://doi.org/10.1029/2008RG000266

Krishnamurthy, V., & Ajayamohan, R. S. (2010). Composite structure of monsoon low pressure systems and its relation to Indian rainfall. *Journal of Climate*, *23*, 4285–4305. https://doi.org/10.1175/2010jcli2953.1

Krishnamurti, T. N., & Ardanuy, P. (1980). 10 to 20-day westward propagating mode and breaks in the monsoons. *Tellus*, *32*, 15–26.

Kummerow, C., Barnes, W., Kozu, T., Shiue, J., & Simpson, J. (1998). The Tropical Rainfall Measuring Mission (TRMM) sensor package. *Journal of Atmospheric and Oceanic Technology*, *15*, 809–817.

Kummerow, C., Simpson, J., Thiele, O., Barnes, W., Chang, A. T. C., Stocker, E., … Nakamura, K. (2000). The status of the Tropical Rainfall Measuring Mission (TRMM) after two years in orbit. *Journal of Applied Meteorology*, *39*, 1965–1982.

Li, C. F., & Yanai, M. (1996). The onset and interannual variability of the Asian summer monsoon in relation to land sea thermal contrast. *Journal of Climate*, *9*, 358–375.

Li, J., & Chen, Y. L. (1998). Barrier jets during TAMEX. *Monthly Weather Review*, *126*, 959–971.

Murata, F., Hayashi, T., Matsumoto, J., & Asada, H. (2007). Rainfall on the Meghalaya Plateau in northeastern India—One of the rainiest places in the world. *Natural Hazards*, *42*, 391–399. https://doi.org/10.1007/s11069-006-9084-z

Murata, F., Terao, T., Hayashi, T., Asada, H., & Matsumoto, J. (2008). Relationship between atmospheric conditions at Dhaka, Bangladesh, and rainfall at Cherrapunjee, India. *Natural Hazards*, *44*, 399–410. https://doi.org/10.1007/s11069-007-9125-2

Nesbitt, S. W., & Anders, A. M. (2009). Very high resolution precipitation climatologies from the Tropical Rainfall Measuring Mission precipitation radar. *Geophysical Research Letters*, *36*, L15815. https://doi.org/10.1029/2009GL038026

Ohsawa, T., Ueda, H., Hayashi, T., Watanabe, A., & Matsumoto, J. (2001). Diurnal variations of convective activity and rainfall in tropical Asia. *Journal of the Meteorological Society of Japan*, *79*, 333–352.

Parish, T. R. (1982). Barrier winds along the Sierra-Nevada Mountains. *Journal of Applied Meteorology*, *21*, 925–930.

Rife, D. L., Pinto, J. O., Monaghan, A. J., Davis, C. A., & Hannan, J. R. (2010). Global distribution and characteristics of diurnally varying low-level jets. *Journal of Climate*, *23*, 5041–5064. https://doi.org/10.1175/2010JCLI3514.1

Romatschke, U., & Houze, R. A. (2011). Characteristics of precipitating convective systems in the South Asian monsoon. *Journal of Hydrometeorology*, *12*, 3–26. https://doi.org/10.1175/2010jhm1289.1

Romatschke, U., Medina, S., & Houze, R. A. (2010). Regional, seasonal, and diurnal variations of extreme convection in the South Asian region. *Journal of Climate*, *23*, 419–439. https://doi.org/10.1175/2009jcli3140.1

Ruchith, R. D., Raj, P. E., Kalapureddy, M. C. R., Deshpande, S. M., & Dani, K. K. (2014). Time evolution of monsoon low-level jet observed over an Indian tropical station during the peak monsoon period from high-resolution Doppler wind lidar measurements. *Journal of Geophysical Research: Atmospheres*, *119*, 1786–1795. https://doi.org/10.1002/2013JD020752

Sato, T. (2013). Mechanism of orographic precipitation around the Meghalaya Plateau associated with intraseasonal oscillation and the diurnal cycle. *Monthly Weather Review*, *141*, 2451–2466. https://doi.org/10.1175/MWR-D-12-00321.1

Shrestha, D., Singh, P., & Nakamura, K. (2012). Spatiotemporal variation of rainfall over the central Himalayan region revealed by TRMM Precipitation Radar. *Journal of Geophysical Research*, *117*, D22106. https://doi.org/10.1029/2012JD018140

Singh, P., & Nakamura, K. (2010). Diurnal variation in summer monsoon precipitation during active and break periods over central India and southern Himalayan foothills. *Journal of Geophysical Research*, *115*, D12122. https://doi.org/10.1029/2009JD012794

Takahashi, H. G., Fujinami, H., Yasunari, T., & Matsumoto, J. (2010). Diurnal rainfall pattern observed by Tropical Rainfall Measuring Mission Precipitation Radar (TRMM-PR) around the Indochina peninsula. *Journal of Geophysical Research*, *115*, D07109. https://doi.org/10.1029/2009JD012155

Tanaka, H., Hiyama, T., Yamamoto, K., Fujinami, H., Shinoda, T., Higuchi, A., … Nakamura, K. (2007). Surface flux and atmospheric boundary layer observations from the LAPS project over the middle stream of the Huaihe River basin in China. *Hydrological Processes*, *21*, 1997–2008. https://doi.org/10.1002/hyp.6706

Terao, T., Islam, M. N., Hayashi, T., & Oka, T. (2006). Nocturnal jet and its effects on early morning rainfall peak over northeastern Bangladesh during the summer monsoon season. *Geophysical Research Letters*, *33*, L18806. https://doi.org/10.1029/2006GL026156

Trenberth, K. E. (1984). Some effects of finite-sample size and persistence on meteorological statistics. Part 1: Autocorrelations. *Monthly Weather Review*, *112*, 2359–2368.

Ueda, H., & Yasunari, T. (1998). Role of warming over the Tibetan Plateau in early onset of the summer monsoon over the Bay of Bengal and South China Sea. *Journal of the Meteorological Society of Japan*, *76*, 1–12.

Van de Wiel, B. J. H., Moene, A. F., Steeneveld, G. J., Baas, P., Bosveld, F. C., & Holtslag, A. A. M. (2010). A conceptual view on inertial oscillations and nocturnal low-level jets. *Journal of the Atmospheric Sciences*, *67*, 2679–2689. https://doi.org/10.1175/2010jas3289.1

Yanase, W., Satoh, M., Taniguchi, H., & Fujinami, H. (2012). Seasonal and intraseasonal modulation of tropical cyclogenesis environment over the Bay of Bengal during the extended summer monsoon. *Journal of Climate*, *25*, 2914–2930. https://doi.org/10.1175/JCLI-D-11-00208.1

Yasunari, T. (1979). Cloudiness fluctuations associated with the Northern Hemisphere summer monsoon. *Journal of the Meteorological Society of Japan*, *57*, 227–242.

Yatagai, A., Arakawa, O., Kamiguchi, K., Kawamoto, H., Nodzu, M. I., & Hamada, A. (2009). A 44-year daily gridded precipitation dataset for Asia based on a dense network of rain gauges. *SOLA*, *5*, 137–140. https://doi.org/10.2151/sola.2009-035

Yatagai, A., Kamiguchi, K., Arakawa, O., Hamada, A., Yasutomi, N., & Kitoh, A. (2012). APHRODITE: Constructing a long-term daily gridded precipitation dataset for Asia based on a dense network of rain gauges. *Bulletin of the American Meteorological Society*, *93*, 1401–1415.